

# INFLUENCE OF GROUND MOTION CHARACTERISTICS ON THE OPTIMAL FRICTION PENDULUM SYSTEM PROPERTIES FOR BASE-ISOLATED STRUCTURES

P. Castaldo<sup>1</sup>, E. Tubaldi<sup>2</sup>

<sup>1</sup> Department of Structural, Geotechnical and Building Engineering (DISEG), Politecnico di Torino, Turin, Italy (corresponding author); Email: [paolo.castaldo@polito.it](mailto:paolo.castaldo@polito.it)

<sup>2</sup> Department of Civil and Environmental Engineering, Imperial College London, London, UK; email: [etubaldi@ic.ac.uk](mailto:etubaldi@ic.ac.uk)

## SUMMARY

This study examines the influence of ground motion characteristics on the optimal friction pendulum (FP) bearings properties for the seismic isolation of structural systems. The evaluation of the optimal FP properties is revisited by considering a non-dimensional formulation which employs the peak ground acceleration (PGA) and the peak ground acceleration-to-velocity (PGA/PGV) ratio as ground motion parameters. A two-degree-of-freedom (2dof) model is employed to describe the isolated system and two different families of records representative respectively of near fault and far field seismic inputs are considered. After carrying out the nondimensionalization of the equation of motion for the proposed ground motion parameters, it is shown that the non-dimensional responses obtained for the two types of seismic inputs are similar. This result confirms that PGA/PGV is a good indicator of the frequency content and of other characteristics of ground motion records, helping to reduce the scatter in the response. Regression expressions are also obtained for the optimal values of the friction coefficient that minimizes the superstructure displacements relative to the base as a function of the abovementioned ground motion parameter and of the dimensionless system parameters. These expression can be used for the preliminary estimation of the optimal FP properties.

**KEYWORDS:** seismic isolation; friction pendulum isolators; non-dimensional form; optimal isolator properties; frequency characteristics of seismic input; PGA/PGV ratio.

## INTRODUCTION

Isolation systems have been extensively implemented for many years to protect structural and non-structural building components from earthquakes and their effectiveness has been demonstrated by a significant number of experimental and numerical studies [1]-[13]. The three basic features common to different isolation devices such as high-damping rubber bearings, lead rubber (LR) bearings, and friction pendulum system (FPS) bearings are horizontal flexibility, necessary to shift the vibration period of the structure away from resonance, energy dissipation capacity, necessary to reduce the displacement demand, and high stiffness at small displacements, required to limit movements due to wind and service loadings.

FP bearings offer some advantages over other bearings, such as the ease of installation, the reduction of displacements at serviceability, the isolation period independent from the system mass [3]-[4]. In single or double concave FP bearings, flexibility is achieved by employing a large radius of curvature of the sliding surface, while the energy dissipation capacity and resistance to service loads depends on the amount of friction provided between the sliding surface and the slider.

In the recent years, increasing research efforts have been devoted to the search of the optimal properties of FP systems. The earliest works employed equivalent spring and damper models to describe the isolation bearing behavior [14]-[15]. Other studies have introduced more advanced models including bi-linear hysteretic ones or models accounting for variation of friction to represent the FP bearings [16]-[20]. These studies provide information useful for the choice of the radius of curvature and friction properties of FP bearing, showing in general that an high energy dissipation

capacity for the isolation system, helpful to reduce the isolator drifts, may increase significantly both the inter-storey drifts and absolute accelerations of the superstructure, thus compromising the benefit of base isolation. Thus, there exists a particular value of the friction coefficient of FPS for which the absolute accelerations or the displacements of the building attain the minimum value. More recent studies have proposed FP design methodologies based on reliability criteria or even life-cycle cost considerations [21]-[25].

While many of these researches have pointed out that the optimum isolation properties are significantly dependent on the ground motion characteristics, very few have analyzed explicitly the relation between the optimal FP isolator properties and the ground motion frequency content. In fact, studies on this issue are rather limited and focused on systems different than those considered in this study. Inaudi and Kelly [26] analyzed a building isolated with bearings exhibiting a visco-elastic behavior showing that the effect of high-frequency content in the excitation is to decrease the optimum viscous damping. Dicleli and Buddaram [27] studied the effect of the frequency characteristics and intensity of the ground motion on the performance of bridges with bilinear isolators. The results of their extensive parametric study demonstrated that the choice of the seismic ground motion according to the characteristics of the bridge site is crucial for a correct design of the isolators. Similar conclusions in the context of isolated bridges have been drawn by [28]-[29].

A recent work of [30] has evaluated the optimal friction of FP isolators for three different sets of artificial records representative of different soil conditions. However, the proposed non-dimensional formulation employed only the spectral acceleration at the fundamental period of the undamped base-isolated structure as ground motion parameter. This parameter does not provide any description of the frequency content of the ground motion and thus it does not allow to unveil the relation between the optimal FP isolator properties and the seismic input characteristics.

This work aims to further advance the study of [30] by proposing an alternative formulation for investigating the influence of the ground motion characteristics on the optimal isolator friction properties. For this purpose, the nondimensionalization of the governing equations of motions proposed in [20] and [30] for the two-degree-of-freedom (2dof) model describing the problem is extended to include an additional ground motion parameter which is equal to the ratio PGA/PGV between the peak ground acceleration (PGA) and the peak ground velocity (PGV) of the input ground motion. This ratio has been shown in many studies to represent synthetically important ground motion features as frequency content and duration [27]-[36] and it has already been employed in previous works analyzing the relation between the seismic input and the optimal isolator properties [27]-[29].

Two different families of ground motions are considered in this study, representing respectively near-fault and far-field seismic records. The near-fault records are also subdivided into three subsets based on their PGA/PGV ratios. Extensive numerical simulations are carried out to evaluate the relation between the structural performance and the characteristic parameters describing the system, the isolator, and the seismic input. Successively, regression expressions are derived for the optimal values of the normalized friction coefficient that minimize the superstructure displacements relative to the base, as a function of the system characteristic parameters and of the frequency content in terms of PGA/PGV. Regression expressions are also derived for the normalized bearing and superstructure displacements corresponding to the optimal friction values. These equations can be very useful for designing the friction properties of the isolators by avoiding the negative consequences of superstructure yielding, which can lead to uncontrolled displacement ductility demand in the superstructure [37]-[39].

## NON-DIMENSIONAL PROBLEM FORMULATION

The equations of motion governing the response of a 2dof model representing an elastic building on single concave FPS isolation bearings (Fig. 1) subjected to the horizontal seismic input  $\ddot{u}_g(t)$  is:

$$\begin{aligned} m_s \ddot{u}_s(t) + c_s \dot{u}_s(t) + k_s u_s(t) &= -m_s [\ddot{u}_g(t) + \ddot{u}_b(t)] \\ m_b \ddot{u}_b(t) + f_b(t) + c_b \dot{u}_b(t) - c_s \dot{u}_s(t) - k_s u_s(t) &= -m_b \ddot{u}_g(t) \end{aligned} \quad (1a,b)$$

where  $u_s$  denotes the displacement of the superstructure relative to isolation bearing,  $u_b$  the isolator (horizontal component) displacement relative to the ground,  $m_s$  and  $m_b$  respectively the mass of the superstructure and of the base floor above the isolation system,  $k_s$  and  $c_s$  respectively the superstructure stiffness and inherent viscous damping constant,  $c_b$  the bearing viscous damping constant,  $t$  the time instant, the dot differentiation over time, and  $f_b(t)$  denotes the FPS bearing resisting force. This latter can be expressed as:

$$f_b(t) = k_b u_b(t) + \mu(\dot{u}_b)(m + m_b) g Z(t) \quad (2)$$

where  $k_b = (m_s + m_b) g / R$ ,  $g$  is the gravity constant,  $R$  is the radius of curvature of the FPS,  $\mu(\dot{u}_b(t))$  the coefficient of sliding friction, which depends on the bearing slip velocity  $\dot{u}_b(t)$ , and  $Z(t) = \text{sgn}(\dot{u}_b)$ , with  $\text{sgn}(\cdot)$  denoting the sign function.

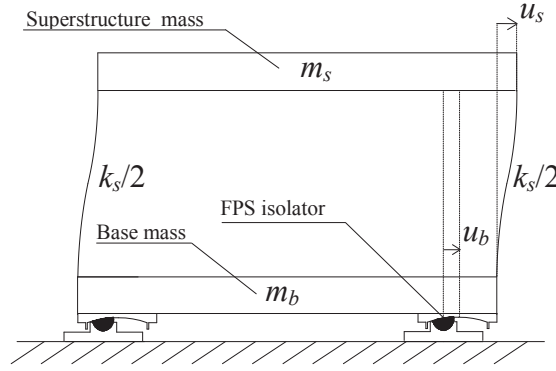


Fig. 1. 2dof model of building isolated with FPS in the deformed configuration.

Experimental results [5]-[7] suggest that the coefficient of sliding friction of Teflon-steel interfaces obeys to the following equation:

$$\mu(\dot{u}_b) = f_{\max} - Df \cdot \exp(-\alpha |\dot{u}_b|) \quad (3)$$

in which  $f_{\max}$  represents the maximum value of friction coefficient attained at large velocities of sliding, and  $f_{\min} = f_{\max} - Df$  represents the value at zero velocity. To further simplify the problem, it is assumed throughout the paper that  $f_{\max} = 3f_{\min}$ ,  $\alpha = 30$  [20], and that the bearing motion is characterized by complete lack of stick-slip tendencies, i.e.,  $Z(t) = \text{sgn}(\dot{u}_b)$  [6].

The non-dimensional form of the equations of motion can be derived by introducing the time and length scales [40]-[44]. The time scale is assumed equal to  $1/\omega_g$ , where  $\omega_g = 2\pi/T_g$  is a circular frequency representative of the frequency content of the ground motion input, as better discussed in the next section. The length scale is assumed as the ratio  $a_0/\omega_g^2$ , where  $a_0$  is a measure of the seismic intensity with the dimension of an acceleration and it is such that  $\ddot{u}_g(t) = a_0 \lambda(\tau)$ , where  $\lambda(\tau)$  is a non-dimensional function of time describing the seismic input time-history. After introducing these scales into Eqn.(1) and rearranging it, the following non-dimensional equations are obtained:

$$\begin{aligned} \ddot{\psi}_s(\tau) + 2\xi_s \frac{\omega_s}{\omega_g} \dot{\psi}_s(\tau) + \frac{\omega_s^2}{\omega_g^2} \psi_s(\tau) &= -[\lambda(\tau) + \dot{\psi}_b(\tau)] \\ \ddot{\psi}_b(\tau) + \frac{1}{1-\gamma} \left[ 2\xi_b \frac{\omega_b}{\omega_g} \dot{\psi}_b(\tau) + \frac{\omega_b^2}{\omega_g^2} \psi_b(\tau) + \frac{\mu(\dot{u}_b)g}{a_0} \text{sgn}(\dot{\psi}_b) \right] &- 2\xi_s \frac{\omega_s}{\omega_g} \frac{\gamma}{1-\gamma} \dot{\psi}_s(\tau) - \frac{\omega_s^2}{\omega_g^2} \frac{\gamma}{1-\gamma} \psi_s(\tau) = -\lambda(\tau) \end{aligned} \quad (4a,b)$$

where  $\omega_s = \sqrt{k_s / m_s}$  and  $\xi_s = c_s / 2m_s \omega_s$  denote respectively the circular frequency and damping factor of the superstructure;  $\omega_b = \sqrt{k_b / (m_s + m_b)} = 2\pi / T_b$  denotes the fundamental circular frequency of the isolated system with infinitely rigid superstructure,  $\xi_b = c_b / 2m_b \omega_b$  the isolator damping factor,  $\gamma = m_s / (m_s + m_b)$  [1] the mass ratio. The non-dimensional parameters  $\psi_s = \frac{u_s \omega_g^2}{a_0}$  and  $\psi_b = \frac{u_b \omega_g^2}{a_0}$  describe the motion of the superstructure and the isolators, respectively.

Eqn.(4) reveals that the non-dimensional parameters ( $\Pi$  terms) [40] that control the system non-dimensional response to the seismic input  $\lambda(\tau)$  are:

$$\Pi_{\omega_s} = \frac{\omega_s}{\omega_b}, \Pi_{\omega_g} = \frac{\omega_b}{\omega_g} = \frac{T_g}{T_b}, \Pi_\gamma = \gamma, \Pi_\mu(\dot{\psi}_b) = \frac{\mu(\dot{u}_b)g}{a_0}, \Pi_{\xi_b} = \xi_b, \Pi_{\xi_s} = \xi_s \quad (5)$$

$\Pi_{\omega_s}$  measures the degree of isolation [20],  $\Pi_{\omega_g}$  is the ratio between the isolator frequency and the circular frequency representative of the ground motion input,  $\Pi_\gamma$  is the previously defined mass ratio,  $\Pi_{\xi_b}$  and  $\Pi_{\xi_s}$  describe the viscous damping inherent respectively to the system and the isolator. Finally,  $\Pi_\mu$  measures the isolator strength, provided by the friction coefficient  $\mu(\dot{u}_b)$ , relative to the seismic intensity. Since this parameter depends on the response through the velocity  $\dot{u}_b$ , the following parameter is used in its stead:

$$\Pi_\mu^* = \frac{f_{\max} g}{a_0} \quad (6)$$

The following set of response parameters relevant to the performance of the isolated system are considered: the peak isolator displacement  $u_{b,\max}$  (important for the design of the FPS isolator and of the seismic gap around the building), and the peak superstructure displacement relative to the isolator  $u_{s,\max}$  (related to internal forces in the structure and to the performance of displacement-sensitive non-structural components). These response parameters can be expressed in non-dimensional form, according to Eqn.(4), as:

$$\psi_{u_b} = \frac{u_{b,\max} \omega_g^2}{PGA}, \psi_{u_s} = \frac{u_{s,\max} \omega_g^2}{PGA} \quad (7a,b)$$

where the normalized displacement response  $\psi_{u_b}$  can be interpreted as the reduction factor of the response spectrum at the isolation period  $T_b$  with damping ratio  $\xi_b=0$ .

The non-dimensional seismic response of the system does not depend on the seismic intensity level  $a_0$ , but it depends only on  $\Pi_{\omega_s}, \Pi_{\omega_g}, \Pi_{\xi_b}, \Pi_{\xi_s}, \Pi_\gamma, \Pi_\mu^*$  and on the function  $\lambda(\tau)$ , describing the frequency content and time-modulation of the seismic input.

It is noteworthy that the absolute accelerations of the superstructure should also be evaluated to monitor the performance of the non-structural components. However, these response quantities are

not considered in this study because the focus of the paper is on the superstructure displacements, which have to be controlled to avoid superstructure yielding. Moreover, previous analyses by the same authors [20] have shown that the 2-sdof system approximation, also adopted in this study, is more accurate when estimating the displacements rather than the accelerations of the superstructure because the displacements are less significantly affected by the contribution of higher order modes.

## SEISMIC INPUT DESCRIPTION

In Eqn.(4), the seismic input is described by the intensity  $a_0$ , which is commonly denoted as seismic intensity measure ( $IM$ ) in the context of the Performance-Based Earthquake Engineering (PBEE), and by the non-dimensional function  $\lambda(\tau)$ , which describes the time-history of the ground motion, and contains the information on the duration of strong shaking and the frequency content. For a given site, these characteristics vary significantly from record to record and they are affected by many variables, including the source-to-site distance, the earthquake magnitude, and the local site conditions. Thus, in the performance assessment of structures more than one record needs to be considered or a stochastic representation of the seismic input must be employed to describe the variability of these characteristics. Although the Response Spectrum or the Fourier Spectrum describe fully an earthquake ground motion, it is often more practical and convenient to characterize it in terms of few parameters. For this reason, many studies have been devoted in the last years to the identification of advanced  $IMs$  capable of synthetically describing the most important features of an earthquake and its effects on structures [45]. In the same context, significant research efforts have been made to define the best scalar measures representing the frequency content of the seismic input. These measures can be used conveniently as time-scales in developing non-dimensional problem formulations for the seismic response assessment of structural systems, as the one described in the previous section [20]. The ratio  $\omega_g = PGA/PGV$  is employed in this work to define the time scale  $1/\omega_g$ . This ratio has been extensively used for analyzing the influence of the ground motion characteristics on the performance of isolated systems [27]-[29] and numerous works have demonstrated that it provides useful information on the frequency content and other characteristics of an input motion [32],[35]. In general, inverse correlation can be found between  $PGA/PGV$  and the magnitude  $M$ , the source to site distance  $R$ , the predominant period of the soil site [34], and also the stochastic bandwidth indicator  $\varepsilon$ , which gives a measure of the frequency band of a random process. Thus, even in the same soil condition, ground motions in the vicinity of small or moderate earthquakes usually have high  $PGA/PGV$  ratios whereas those distant from large earthquakes usually have low  $PGA/PGV$  ratios. Results of seismological studies are often available that allow to estimate the probability distribution of  $PGA/PGV$  at a site [36]. For these reasons, the  $PGA/PGV$  has been preferred for this study to other time scales commonly employed in the literature such as the predominant period of the ground motion  $T_m$  [40]-[44]. However, it should be observed that a strong inverse correlation is found between  $PGA/PGV$  and  $T_m$  [35]. Thus, these measures are equally good for describing the characteristics of the ground motion input. In this study, two different types of records are considered. The first set consists of 45 far field (FF) records which have been widely used for studies of the effect of the  $PGA/PGV$  ratio on the response of structures. These records are subdivided into three subsets based on their  $PGA/PGV$  ratios (high, medium or low), with 15 records in each subset, as reported in Tables 1-3. Usually, high  $PGA/PGV$  ratios are associated with records of short duration and high energy content in the high frequency range, whereas low  $PGA/PGV$  ratios denote records with long duration and high energy content in the low frequency range [30]-[33]. Thus, low  $PGA/PGV$  ratios are expected to be more critical for isolated systems such as the one considered.

The second set of records consists of 40 near fault (NF) ground motions, whose characteristics are reported in Table 4. This set of records has been included in the study to investigate whether the proposed ground motion parameters and non-dimensional formulation are capable of describing the essential characteristics of the seismic input and provide a non-dimensional response which is not

strongly affected by the type of records considered. As expected, on average the NF records are characterized by low PGA/PGV ratios, below 0.8g. Only in one case a high value of PGA/PGV, higher than 1g, is observed.

Table 1. Subset of far-field records corresponding to high PGA/PGV values [PGA(g)/PGV>1.2]

Earthquake	Date	Magn.	Site	Epic. Dist. (km)	Comp.	PGA(g)	PGV (m/s)	PGA(g)/PGV	Soil
Parkfield California	June 27 1966	5.6	Temblor No. 2	7	N65W	0.269	0.145	1.86	Rock
Parkfield California	June 27 1966	5.6	Cholame, Shandon No. 5	5	N85W	0.434	0.255	1.7	Rock
San Francisco California	Mar. 22 1957	5.25	Golden Gate Park	11	S80E	0.105	0.046	2.28	Rock
San Francisco California	Mar. 22 1957	5.25	State Bldg., S.F.	17	S09E	0.085	0.051	1.67	Stiff Soil
Helena Montana	Oct. 31 1935	6	Carroll College	8	N00E	0.146	0.072	2.03	Rock
Lytle Creek	Sep. 12 1970	5.4	Wrightwood, California	15	S25W	0.198	0.096	2.06	Rock
Oroville California	Aug. 1 1975	5.7	Seismogr. Station Oroville	13	N53W	0.084	0.044	1.91	Rock
San Fernando California	Feb. 9 1971	6.4	Pacomia Dam	4	S74W	1.075	0.577	1.86	Rock
San Fernando California	Feb. 9 1971	6.4	Lake Hughes, Station 4	26	S21W	0.146	0.085	1.72	Rock
Nahanni N.W.T., Canada	Dec. 23 1985	6.9	Site 1, Iverson	7.5	LONG	1.101	0.462	2.38	Rock
Central Honshu Japan	Feb. 26 1971	5.5	Yoneyama Bridge	27	TRANS	0.151	0.059	2.56	Stiff Soil
Near E. Coast of Honshu	May. 11 1972	5.8	Kushiro Central Wharf	33	N00E	0.146	0.06	2.43	Stiff Soil
Honshu Japan	Apr. 5 1966	5.4	Hoshina-A	4	N00E	0.27	0.111	2.43	Stiff Soil
Monte Negro Yugoslavia	Apr. 9 1979	5.4	Albatros Hotel, Ulcinj	12.5	N00E	0.042	0.016	2.63	Rock
Banja Luka Yugoslavia	Aug. 13 1981	6.1	Seism. Station, Banja	8.5	N90W	0.074	0.032	2.31	Rock

Table 2. Subset of far-field records corresponding to intermediate PGA(g)/PGV values [0.8<PGA(g)/PGV<1.2]

Earthquake	Date	Magn.	Site	Epic. Dist. (km)	Comp.	PGA(g)	PGV (m/s)	PGA(g)/PGV	Soil
Imperial Valley California	May 18 1940	6.6	El Centro	8	S00E	0.348	0.334	1.04	Stiff Soil
Kern County California	July 21 1952	7.6	Taft Lincoln School Tunnel	56	S69E	0.179	0.177	1.01	Rock
Kern County California	July 21 1952	7.6	Taft Lincoln School Tunnel	56	N21E	0.156	0.157	0.99	Rock
Borrego Mtn. California	April 8 1968	6.5	San Onofre SCE Power Plant	122	N57W	0.046	0.042	1.1	Stiff Soil
Borrego Mtn. California	April 8 1968	6.5	San Onofre SCE Power Plant	122	N33E	0.041	0.037	1.11	Stiff Soil
San Fernando California	Feb. 9 1971	6.4	3838 Lankershim Blvd., L.A.	24	S90W	0.15	0.149	1.01	Rock
San Fernando California	Feb. 9 1971	6.4	Hollywood Storage P.E. Lot, L.A.	35	N90E	0.211	0.211	1	Stiff Soil
San Fernando California	Feb. 9 1971	6.4	3407 6 <sup>th</sup> Street, L.A.	39	N90E	0.165	0.166	0.99	Stiff Soil
San Fernando California	Feb. 9 1971	6.4	Griffith Park Observatory, L.A.	31	S00W	0.18	0.205	0.88	Rock
San Fernando California	Feb. 9 1971	6.4	234 Figueroa St., L.A.	41	N37E	0.199	0.167	1.19	Stiff Soil
Near East Coast of	Nov. 16 1974	6.1	Kashima Harbor Works	38	N00E	0.07	0.072	0.97	Stiff Soil
Near East Coast of	Aug. 2 1971	7	Kushiro Central Wharf	196	N90E	0.078	0.068	1.15	Stiff Soil
Monte Negro Yugoslavia	Apr. 15 1979	7	Albatros Hotel, Ulcinj	17	N00E	0.171	0.194	0.88	Rock
Mexico Earthq.	Sept. 19 1985	8.1	El Suchil, Guerrero Array	230	S00E	0.105	0.116	0.91	Rock
Mexico Earthq.	Sept. 19 1985	8.1	La Villita, Guerrero Array	44	N90E	0.123	0.105	1.17	Rock

Table 3. Subset of far-field records corresponding to low PGA(g)/PGV values [PGA(g)/PGV<0.8]

Earthquake	Date	Magn.	Site	Epic. Dist. (km)	Comp.	PGA(g)	PGV (m/s)	PGA(g)/PGV	Soil
Long Beach California	Mar. 10 1933	6.3	Subway Terminal, L.A.	59	N51W	0.097	0.237	0.41	Rock
Long Beach California	Mar. 10 1933	6.3	Subway Terminal, L.A.	59	N39E	0.064	0.173	0.37	Rock
Lower Calif.	Dec. 30 1934	6.5	El Centro	58	S00W	0.16	0.209	0.77	Stiff Soil
San Fernando California	Feb. 9 1971	6.4	2500 Wilshire Blvd., L.A.	40	N61W	0.101	0.193	0.52	Stiff Soil
San Fernando California	Feb. 9 1971	6.4	3550 Wilshire Blvd., L.A.	39	WEST	0.132	0.216	0.61	Stiff Soil
San Fernando California	Feb. 9 1971	6.4	222 Figueroa St., L.A.	41	S37W	0.129	0.186	0.69	Stiff Soil
San Fernando California	Feb. 9 1971	6.4	3470 Wilshire Blvd., L.A.	39	S90W	0.114	0.186	0.61	Stiff Soil
San Fernando California	Feb. 9 1971	6.4	4680 Wilshire Blvd., L.A.	38	N15E	0.117	0.215	0.54	Stiff Soil
San Fernando California	Feb. 9 1971	6.4	445 Figueroa St., L.A.	41	S38W	0.119	0.173	0.69	Rock
San Fernando California	Feb. 9 1971	6.4	Hollywood Storage L.A.	32	S00W	0.106	0.17	0.62	Stiff Soil
Near E. Coast of Honshu,	May 16 1968	7.9	Muroran Harbor	290	N00E	0.226	0.334	0.68	Stiff Soil
Near E. Coast of Honshu,	June 17 1973	7.4	Kushiro Central Wharf	112	N00E	0.205	0.275	0.75	Stiff Soil
Mexico Earthq.	Sep. 19 1985	8.1	Zihuatenejo, Guerrero Array	135	S00E	0.103	0.159	0.65	Rock
Mexico Earthq.	Sep. 19 1985	8.1	Teacalco, Cuerrero Array	333	N00E	0.052	0.074	0.7	Rock
Mexico Earthq.	Sep. 19 1985	8.1	Mesa Vibradora C.U., Mexico City	379	N90W	0.04	0.11	0.36	Rock

Records with the same PGA/PGV ratio may have different effect on the analyzed system, depending on the influence of those features of the ground motion that PGA/PGV is not able to describe. Thus, despite the normalization by the time scale  $1/\omega_g$ , some dispersion is expected in the normalized response. Obviously, the dispersion would be zero in the case of a harmonic input with circular frequency  $\omega_g$ . To prove this, the first record of the far-field subset with high PGA/PGV ( $T_g = 2\pi/\omega_g = 0.34$  s) and the first record of the subset with low PGA/PGV ( $T_g = 2\pi/\omega_g = 1.56$ s) are considered. Two systems, each characterized by the same normalized parameters  $T_b = 2T_g$ ,  $\Pi_{\omega_s} = 6$ ,

$\Pi_{\xi_b}=2\%$ ,  $\Pi_{\xi_s}=2\%$ ,  $\Pi_{\gamma}=0.7$ ,  $\Pi_{\mu}^*=0.05$ , are subjected to these two records. The same systems are also subjected to two harmonic inputs with period  $T_g$  equal to that of the two records. The normalized time-histories of the displacement, shown in Fig. 2, are coincident for the harmonic inputs, whereas they differ for the ground motion records and this demonstrates that despite the normalization, different results are obtained for each of the records of the three sets.

Table 4. Near fault records.

Earthquake	Year	Magn.	Site	Closest dist. (km)	Comp.	PGA(g)	PGV (m/s)	PGA(g)/PGV	Soil type
Imperial Valley-06	1979	6.53	Subway Terminal, L.A.	7.31	SN	0.180	0.545	0.33	C
Imperial Valley-06	1979	6.53	Subway Terminal, .A.	0.07	SN	0.378	1.150	0.33	C
Imperial Valley-06	1979	6.53	El Centro	7.05	SN	0.357	0.779	0.46	C
Imperial Valley-06	1979	6.53	El Centro	3.95	SN	0.375	0.915	0.41	C
Imperial Valley-06	1979	6.53	El Centro	1.35	SN	0.442	1.119	0.39	C
Imperial Valley-06	1979	6.53	El Centro	0.56	SN	0.462	1.088	0.42	C
Imperial Valley-06	1979	6.53	El Centro	3.86	SN	0.468	0.486	0.96	C
Imperial Valley-06	1979	6.53	El Centro	5.09	SN	0.417	0.596	0.70	C
Morgan Hill	1984	6.19	El Centro	0.53	SN	0.814	0.623	1.31	B
Loma Prieta	1989	6.93	El Centro	9.96	SN	0.294	0.308	0.95	B
Loma Prieta	1989	6.93	El Centro	3.88	SN	0.944	0.970	0.97	B
Landers	1992	7.28	El Centro	2.19	SN	0.704	1.406	0.50	B
Landers	1992	7.28	El Centro	23.62	SN	0.236	0.566	0.42	C
Northridge-01	1994	6.69	El Centro	5.43	SN	0.617	0.674	0.92	B
Northridge-01	1994	6.69	El Centro	5.43	SN	0.518	0.674	0.77	B
Northridge-01	1994	6.69	El Centro	5.92	SN	0.724	1.203	0.60	C
Northridge-01	1994	6.69	El Centro	5.48	SN	0.426	0.878	0.49	C
Northridge-01	1994	6.69	El Centro	6.5	SN	0.870	1.672	0.52	C
Northridge-01	1994	6.69	El Centro	5.35	SN	0.594	1.303	0.46	C
Northridge-01	1994	6.69	El Centro	5.19	SN	0.828	1.136	0.73	B
Northridge-01	1994	6.69	El Centro	5.3	SN	0.733	1.227	0.60	B
Kobe, Japan	1995	6.9	El Centro	0.96	SN	0.854	0.963	0.89	C
Kobe, Japan	1995	6.9	El Centro	0.27	SN	0.645	0.726	0.89	C
Kocaeli, Turkey	1999	7.51	El Centro	10.92	SN	0.241	0.512	0.47	B
Chi-Chi, Taiwan	1999	7.62	El Centro	3.14	SN	0.664	0.777	0.85	B
Chi-Chi, Taiwan	1999	7.62	El Centro	9.96	SN	0.383	0.753	0.51	C
Chi-Chi, Taiwan	1999	7.62	El Centro	3.78	SN	0.286	0.461	0.62	B
Chi-Chi, Taiwan	1999	7.62	El Centro	0.66	SN	0.375	1.655	0.23	B
Chi-Chi, Taiwan	1999	7.62	El Centro	5.97	SN	0.224	0.409	0.55	B
Chi-Chi, Taiwan	1999	7.62	El Centro	5.3	SN	0.157	0.604	0.26	B
Chi-Chi, Taiwan	1999	7.62	3470 WilshireBlvd., L.A.	0.32	SN	0.564	1.846	0.31	B
Chi-Chi, Taiwan	1999	7.62	4680 WilshireBlvd., L.A.	0.91	SN	0.331	0.886	0.37	B
Chi-Chi, Taiwan	1999	7.62	445 Figueroa St., L.A.	2.76	SN	0.310	0.678	0.46	B
Chi-Chi, Taiwan	1999	7.62	Hollywood Storage L.A.	5.18	SN	0.235	0.578	0.41	B
Chi-Chi, Taiwan	1999	7.62	Muroan Harbor	7	SN	0.127	0.437	0.29	B
Chi-Chi, Taiwan	1999	7.62	Kushiro Central Wharf	2.13	SN	0.212	0.684	0.31	C
Chi-Chi, Taiwan	1999	7.62	Zihuatenejo, Guerrero Array	1.51	SN	0.295	1.090	0.27	B
Chi-Chi, Taiwan	1999	7.62	Teacalco, Cuerrero Array	6.1	SN	0.133	0.621	0.21	B
Chi-Chi, Taiwan	1999	7.62	Teacalco, Cuerrero Array	9.35	SN	0.224	0.424	0.53	B
Chi-Chi, Taiwan	1999	7.62	Mesa VibradoraC.U., Mexico	9.96	SN	0.303	0.676	0.45	C

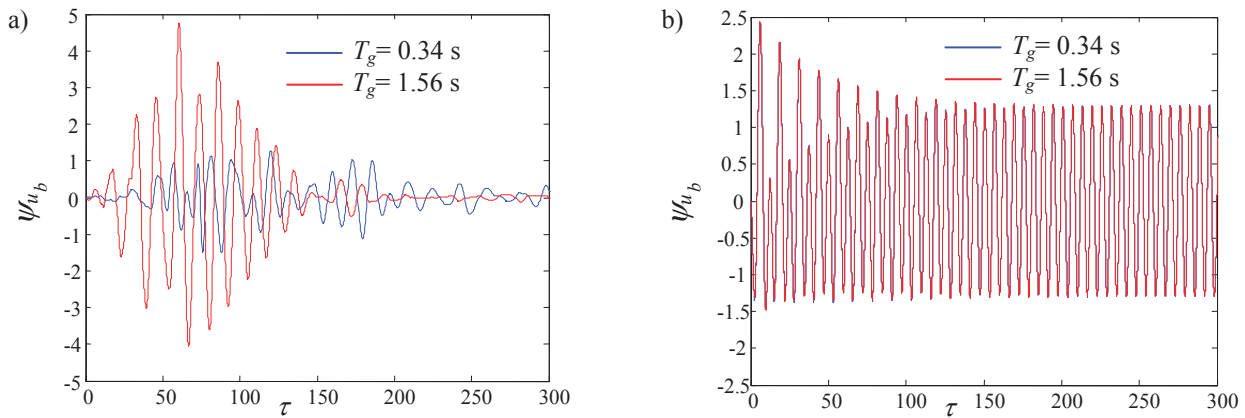


Fig. 2. Normalized response of two systems with the same characteristic parameters subjected to two natural records (a) and two harmonic inputs (b) with  $T_g=0.34s$  and  $T_g=1.56s$ .

## PARAMETRIC STUDY

This section illustrates the parametric study carried out to evaluate the relation among the isolation and structure properties, the seismic input frequency content, and the probabilistic response. The parameters  $\Pi_{\xi_b} = \xi_b$  and  $\Pi_{\xi_s} = \xi_s$  are both assumed equal to 2%, the parameter  $\Pi_{\omega_s}$  is varied in the range between 3 (flexible superstructure) and 12 (rigid superstructure),  $\Pi_{\gamma} = \gamma$  in the range between 0.6 and 0.9,  $\Pi_{\mu}^*$  in the range between 0 (no friction) and 2 (very high friction), and  $T_b/T_g$  is varied in the range between 0 and 16. It is noteworthy that the range of variation assumed for  $T_b/T_g$  is very wide, and that in design practice values of  $T_b/T_g$  higher than unity are usually observed since  $T_b$  is usually equal or higher than 2s for isolated systems, and  $T_g$  is smaller than unity.

The probabilistic response is evaluated by considering separately the set of far field records (for a total of 45 ground motions) and the set of near fault records (40 ground motions). The Runge–Kutta–Fehlberg integration algorithm available in Matlab-Simulink [56] is employed to solve Eqn.(4) for each value of the parameters varied in the parametric study and for the different ground motion considered. By assuming that the response parameters follow a lognormal distribution [20], only the first two moments of the response need to be estimated to determine the response statistic. The lognormal distribution can be fitted to the generic response parameter  $D$  (i.e., the extreme values  $\psi_{u_b}$ ,  $\psi_{u_s}$  of Eq. (7)) by estimating the sample geometric mean,  $GM(D)$ , and the sample lognormal standard deviation  $\sigma_{\ln}(D)$ , or dispersion  $\beta(D)$ , defined as follows:

$$GM(D) = \sqrt[N]{d_1 \cdot \dots \cdot d_N} \quad (8)$$

$$\beta(D) = \sigma_{\ln}(D) = \sqrt{\frac{(\ln d_1 - \ln[GM(D)])^2 + \dots + (\ln d_N - \ln[GM(D)])^2}{N-1}} \quad (9)$$

where  $d_i$  denotes the  $i$ -th sample value of  $D$ , and  $N$  is the total number of samples. The sample geometric mean is an estimator of the median of the response and its logarithm coincides with the lognormal sample mean  $\mu_{\ln}(D)$ . Under the lognormality assumption, the  $k$ th percentile of the generic response parameter  $D$  can be expressed in function of the geometric mean  $GM(D)$  and of the dispersion  $\beta(D)$  as:

$$d_k = GM(D) \exp[f(k)\beta(D)] \quad (10)$$

where  $f(k)$  is a function assuming the values  $f(50) = 0$ ,  $f(84) = 1$  and  $f(16) = -1$  [57].

### *Results obtained for the FF record set*

This subsection illustrates the results obtained for the FF record set. Figs. 3-8 show the statistics ( $GM$  and  $\beta$  values) of the response parameters considered, obtained for different values of the system parameters varying in the range of interest. In particular, Figs. 3 and 4 report the results concerning the normalized bearing displacement  $\psi_{u_b}$  for the four values of  $\Pi_{\omega_s}$ . In general,  $GM(\psi_{u_b})$  is zero for  $T_b/T_g = 0$ , it increases for increasing  $T_b/T_g$  and then it decreases, by following a trend similar to that of a displacement response spectrum of a sdof system with respect to the system vibration period. Obviously,  $GM(\psi_{u_b})$  decreases significantly as  $\Pi_{\mu}^*$  increases. The values of  $GM(\psi_{u_b})$  are only slightly influenced by  $\Pi_{\gamma}$  and  $\Pi_{\omega_s}$ . In particular,  $GM(\psi_{u_b})$  increases slightly for increasing isolation degree. These results are in agreement with those of other studies

which have shown that seismic isolation is more effective for firm or rock type soil than the soft soils [30].

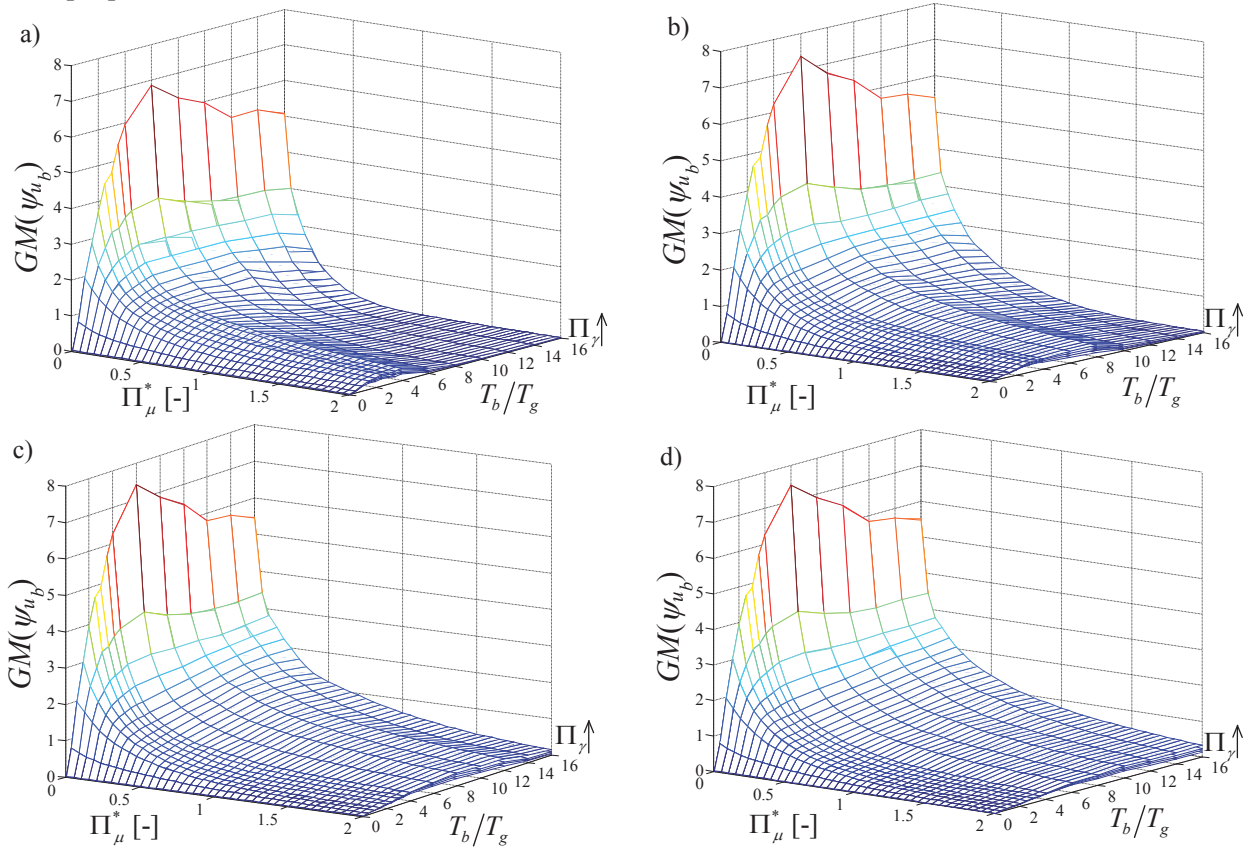


Fig. 3. Normalized bearing displacement vs.  $\Pi_\mu^*$  and  $T_b/T_g$ : median value for  $\Pi_{os}=3$  (a),  $\Pi_{os}=6$  (b),  $\Pi_{os}=9$  (c) and  $\Pi_{os}=12$  (d) for different values of  $\Pi_\gamma$ . The arrow denotes the increasing direction of  $\Pi_\gamma$ . FF record set.

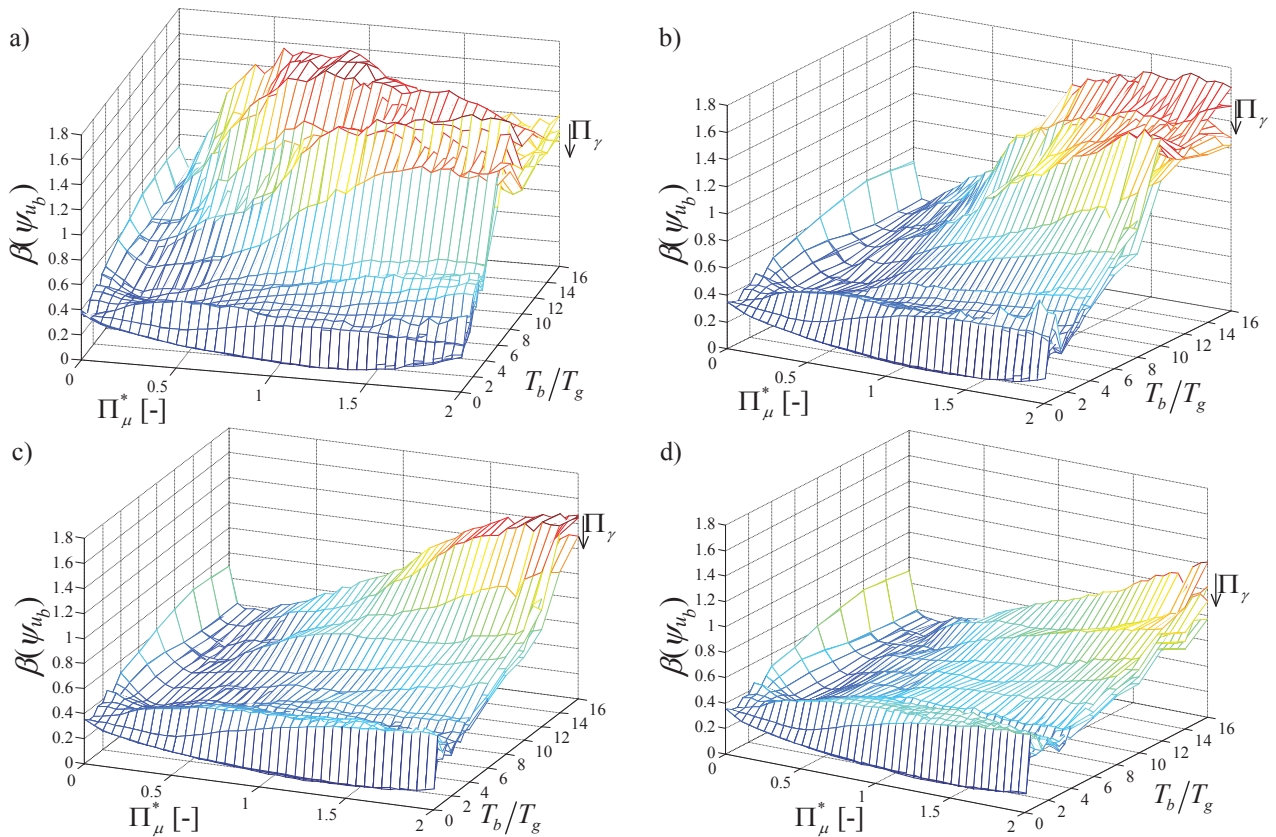


Fig. 4. Normalized bearing displacement vs.  $\Pi_\mu^*$  and  $T_b/T_g$ : dispersion for  $\Pi_{os}=3$  (a),  $\Pi_{os}=6$  (b),  $\Pi_{os}=9$  (c) and  $\Pi_{os}=12$  (d) for different values of  $\Pi_\gamma$ . The arrow denotes the increasing direction of  $\Pi_\gamma$ . FF record set.

The dispersion  $\beta(\psi_{u_b})$  is also in general quite low for all the values of the system and FPS characteristic parameters. This demonstrates on one hand the efficiency of the proposed normalization approach and of the time and length scales adopted, and on the other hand the fact that the PGA is not an efficient seismic intensity measure for the problem at hand [45]. In fact, the knowledge of the PGA only does not permit to achieve a confident estimate of the isolator response, which is significantly influenced by the parameter  $T_b/T_g$ . Thus, the parameter  $T_g$  can be also considered as an additional ground motion parameter to be in conjunction with PGA to form a vector-valued *IM*. It is also worth to note that  $T_g$  exhibits a significant correlation and can be expressed in function of other ground motion parameters such as  $M$  and  $R$  usually considered for evaluating the sufficiency of an *IM* [58].

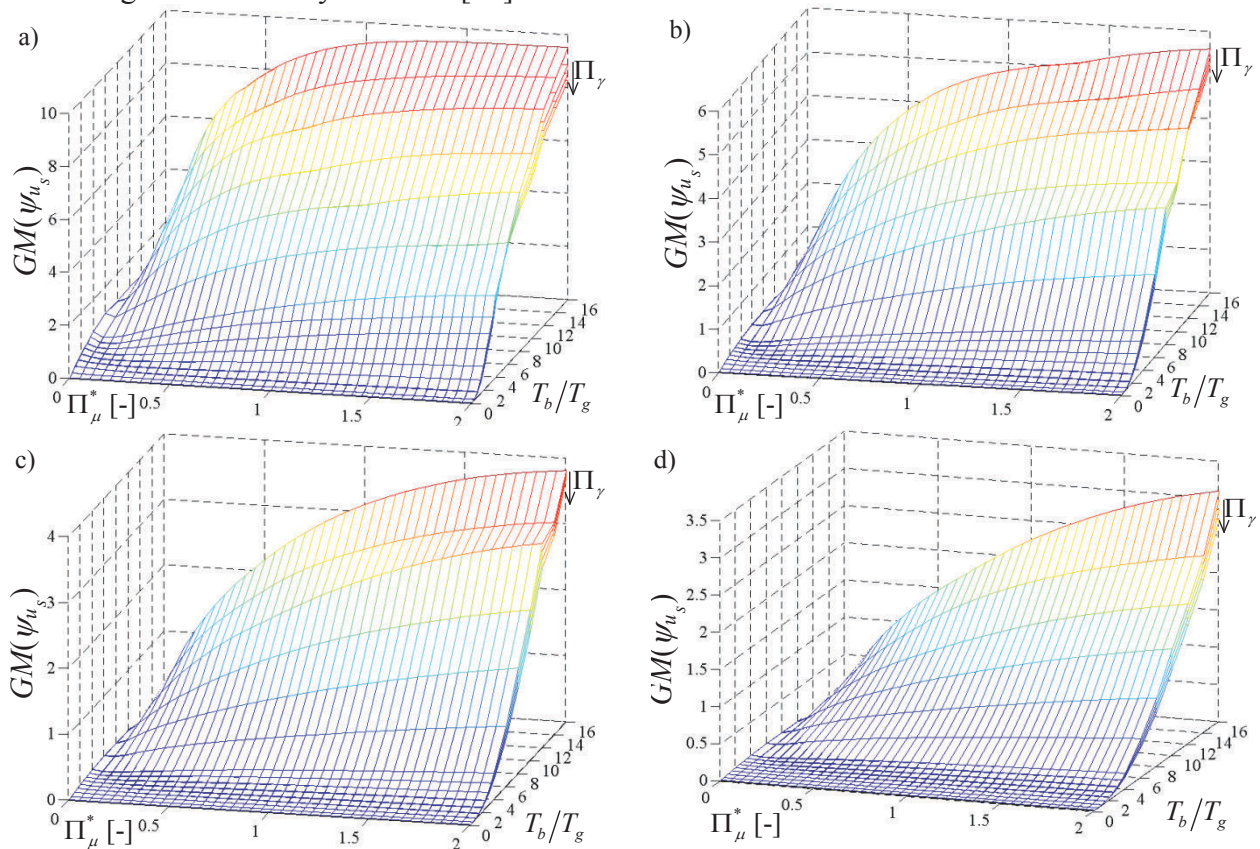


Fig. 5. Normalized superstructure displacement vs.  $\Pi_\mu^*$  and  $T_b/T_g$ : median value for  $\Pi_{os}=3$  (a),  $\Pi_{os}=6$  (b),  $\Pi_{os}=9$  (c) and  $\Pi_{os}=12$  (d) for different values of  $\Pi_\gamma$ . The arrow denotes the increasing direction of  $\Pi_\gamma$ . FF record set.

Fig. 5 shows the variation with the system parameters of the geometric mean of the normalized superstructure displacement  $GM(\psi_{u_s})$  relative to the base mass. The results obtained for the different values of  $\Pi_{os}$  are reported in separate figures, as this parameter influences the superstructure response. In general, it is observed that  $GM(\psi_{u_s})$  increases for increasing values of  $T_b/T_g$  whereas it first decreases, and then increases for increasing values of  $\Pi_\mu^*$ . Thus, there exists a value of  $\Pi_\mu^*$ , which is denoted as optimal, which minimizes  $GM(\psi_{u_s})$ . This optimal value strongly depends on the values assumed by the system parameters, especially, on  $T_b/T_g$  ratio. Moreover,  $GM(\psi_{u_s})$  decreases for increasing isolation degree. The values of the dispersion,  $\beta(\psi_{u_s})$ , represented in Fig. 6, are in general very low and smaller than the corresponding values for the normalized bearing displacement. Moreover, the dispersion of  $\psi_{u_s}$  is also minimized by the

optimal value of  $\Pi_\mu^*$  which minimizes the geometric mean of  $\psi_{u_s}$ . The existence of an optimal value of the friction coefficient has been pointed out in many studies on systems isolated by FPS bearings [20],[15]-[18],[30] and it is the result of two counteracting effects that follow an increase of the friction coefficient. The first effect is the increase of isolator strength, with associated increase of forces transferred to the superstructure. The second effect is an increase of energy dissipation and a reduction of the bearing displacements, which also influence the forces transferred to the superstructure.

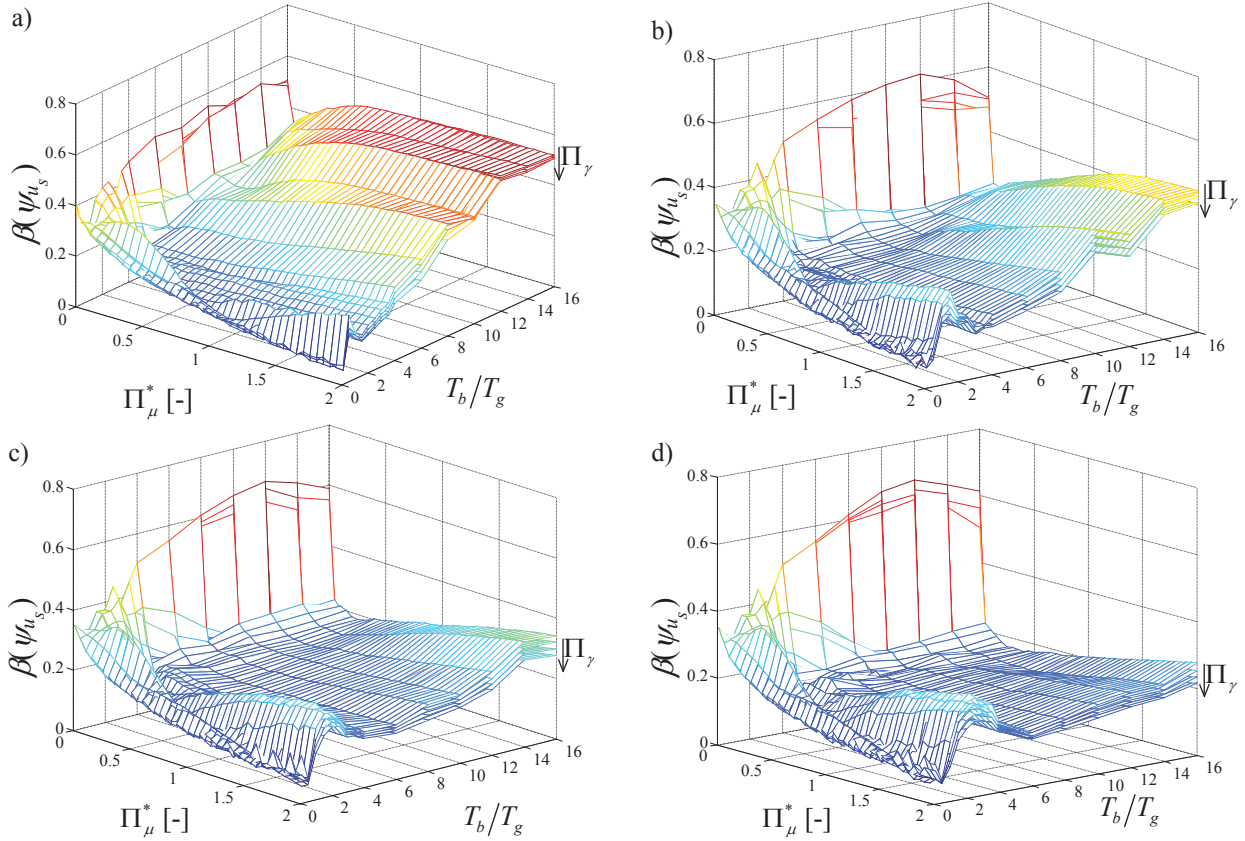
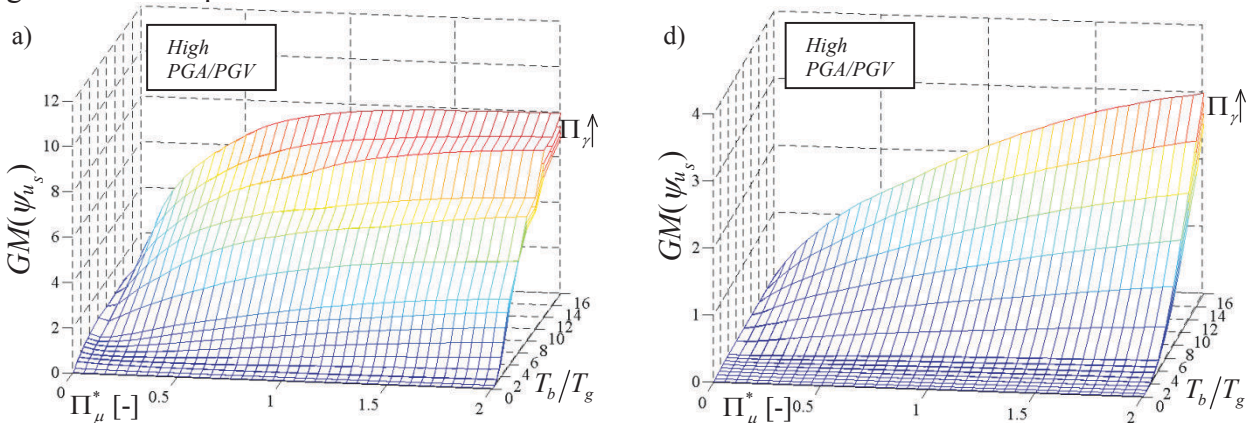


Fig. 6. Normalized superstructure displacement vs.  $\Pi_\mu^*$  and  $T_b/T_g$ : dispersion for  $\Pi_{os}=3$  (a),  $\Pi_{os}=6$  (b),  $\Pi_{os}=9$  (c) and  $\Pi_{os}=12$  (d) for different values of  $\Pi_\gamma$ . The arrow denotes the increasing direction of  $\Pi_\gamma$ . FF record set.

Fig. 7 shows the variation of the median values of the superstructure displacement obtained by considering separately the three different subsets of FF records, characterized by different ranges of PGA/PGV values. The observed trends observed for the different PGA/PGV ranges are very close, or in other terms the median responses obtained for the three records subsets for a given combination of  $\Pi_\gamma$ ,  $\Pi_{os}$  and of  $T_b/T_g$  values are statistically not different. This confirms that the normalized response is not significantly affected by the record selection if  $T_g$  is considered as ground motion parameter.



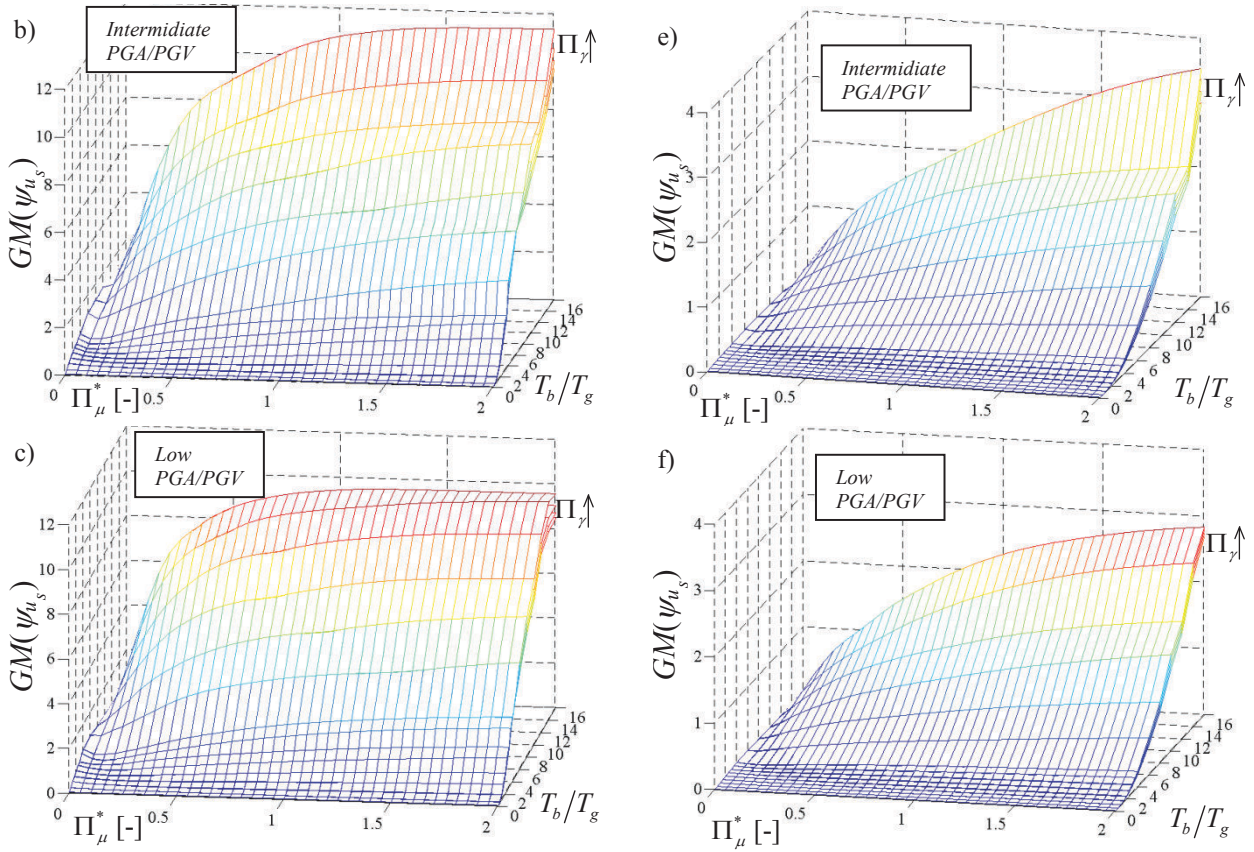


Fig. 7. Normalized superstructure displacement vs.  $\Pi_\mu^*$  and  $T_b/T_g$ : median values for  $\Pi_{os}=3$  (a,b,c) and  $\Pi_{os}=12$  (d,e,f) for different values of  $\Pi_\gamma$ , for the three different subsets of far-field records. The arrow denotes the increasing direction of  $\Pi_\gamma$ .

### Results obtained for the NF record set

This subsection illustrates the results obtained for the NF record set. In particular, Figs.8 and 9 show the statistics of the isolator displacement and Figs.10 and 11 show the statistics of the superstructure displacement, for the different values of  $\Pi_{os}$ ,  $\Pi_\gamma$  and of  $T_b/T_g$ . The observed trends are very similar to those obtained for the FF records. This again confirms the importance of accounting for  $T_b/T_g$  in evaluating the system performance and the fact that when  $T_g$  is used as indicator of the frequency content of the seismic input, the normalized response does not depend significantly on other characteristics of the seismic input.

For a given value of  $\Pi_{os}$ ,  $\Pi_\gamma$  and of  $T_b/T_g$ , the normalized median responses of the isolation system and of the superstructure under the FF ground motions are higher than the corresponding responses under the NF ground motions. This result is very interesting and only apparently contradicts the conclusions of other studies for which NF records are more demanding for isolated systems than FF records (e.g. [59],[60]). In fact, NF records are demanding for isolated systems because they are characterized by a higher energy content at low frequencies compared to FF records. However, this feature is already taken into account in this study by the parameter  $T_b/T_g$ . For the same  $T_b/T_g$  value, FF records may induce higher displacement demands because differently from NF records they are characterized by multiple cycles of large amplitudes rather than a single pulse. The work of Chopra and Chintanapakdee [61] has already demonstrated the importance of the number of large amplitude cycles on the maximum seismic response.

Moreover, the results reported in Fig.10 show that, as in the case of FF records, there exists an optimal value of the normalized friction that minimize the superstructure median response.

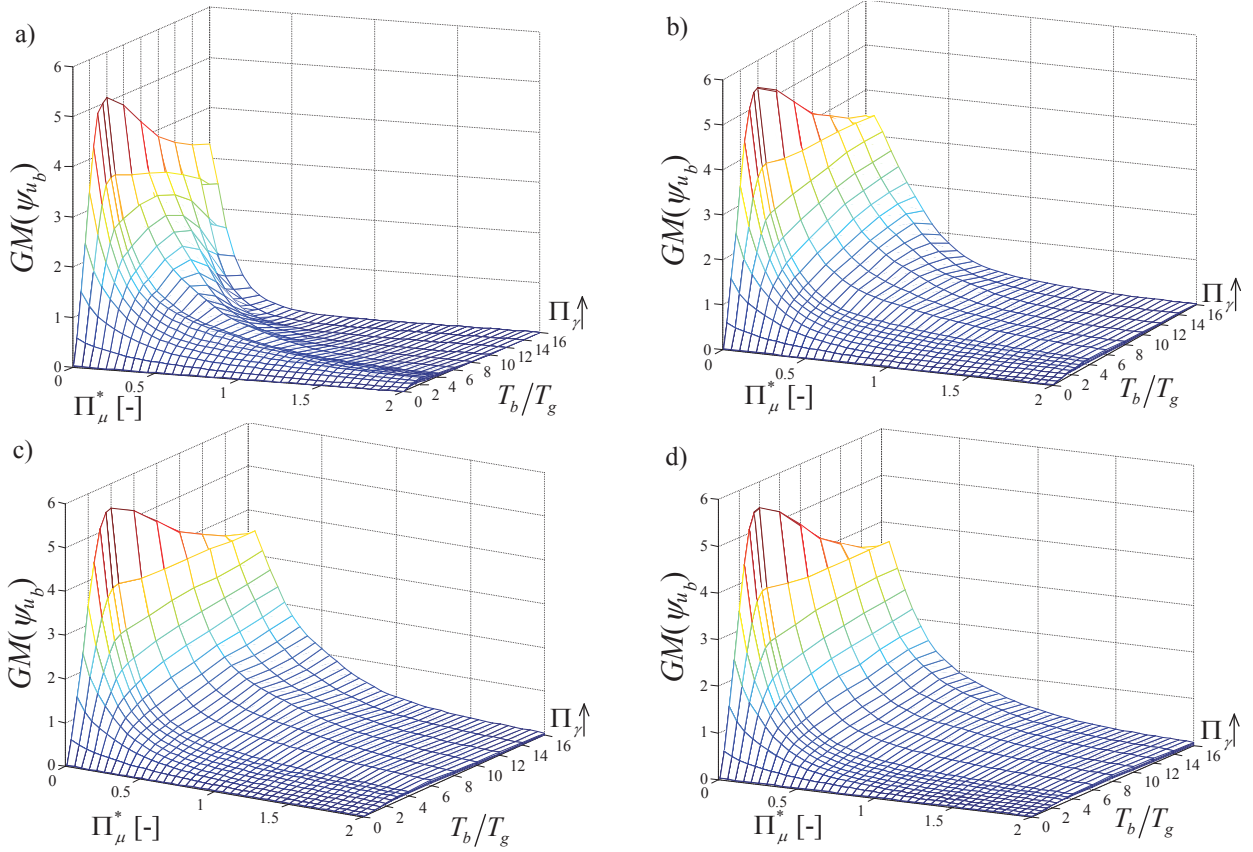


Fig. 8. Normalized bearing displacement vs.  $\Pi_\mu^*$  and  $T_b/T_g$ : median value for  $\Pi_{os}=3$  (a),  $\Pi_{os}=6$  (b),  $\Pi_{os}=9$  (c) and  $\Pi_{os}=12$  (d) for different values of  $\Pi_\gamma$ . The arrow denotes the increasing direction of  $\Pi_\gamma$ . NF record set.

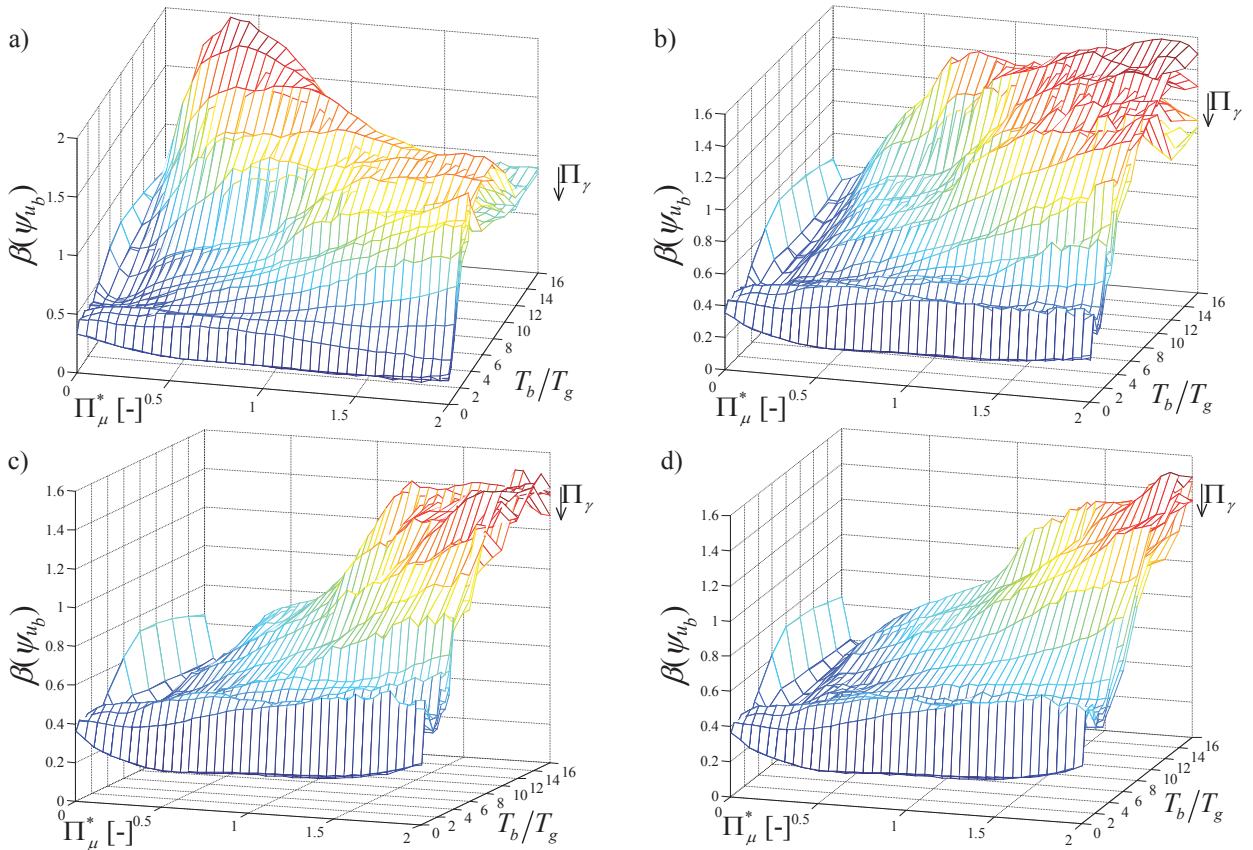


Fig. 9. Normalized bearing displacement vs.  $\Pi_\mu^*$  and  $T_b/T_g$ : dispersion for  $\Pi_{os}=3$  (a),  $\Pi_{os}=6$  (b),  $\Pi_{os}=9$  (c) and  $\Pi_{os}=12$  (d) for different values of  $\Pi_\gamma$ . The arrow denotes the increasing direction of  $\Pi_\gamma$ . NF record set.

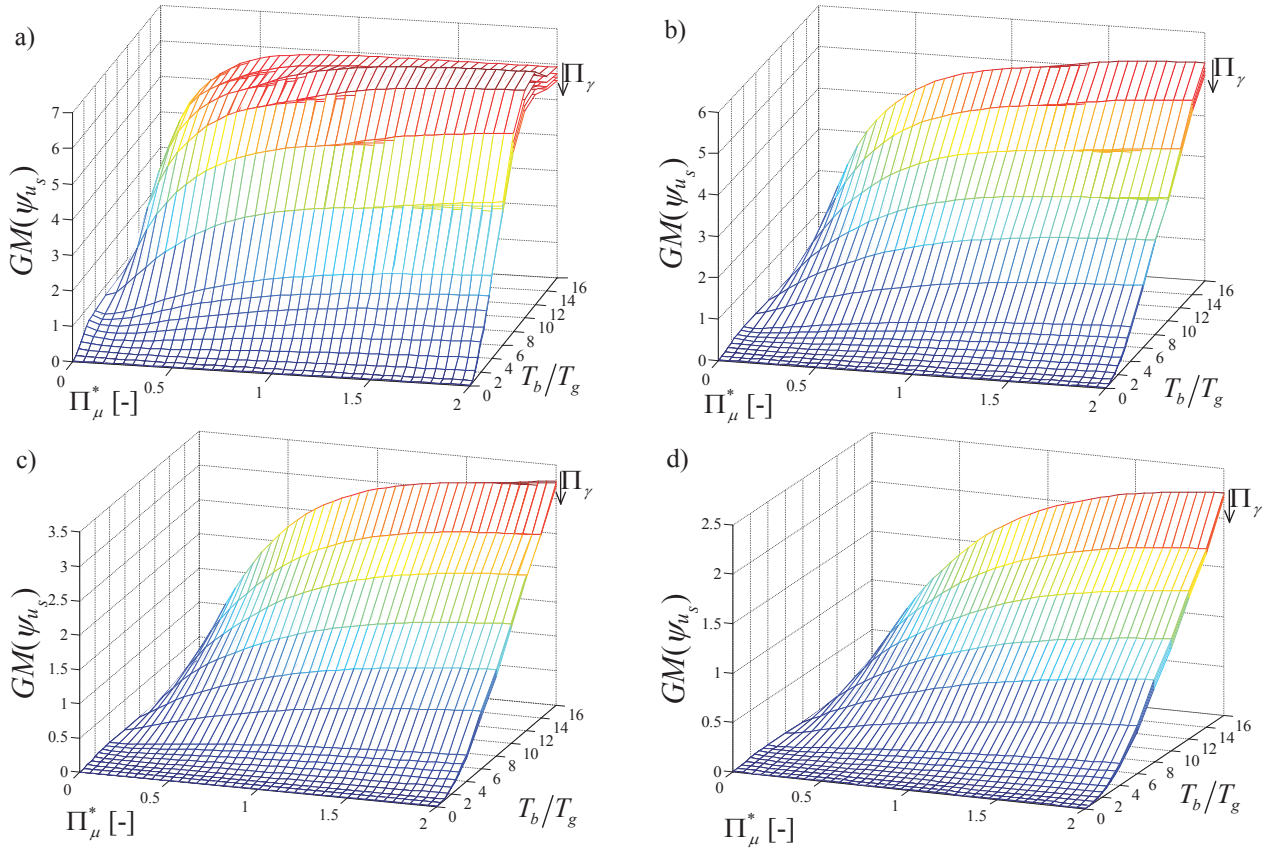


Fig. 10. Normalized superstructure displacement vs.  $\Pi_\mu^*$  and  $T_b/T_g$ : median value for  $\Pi_{os}=3$  (a),  $\Pi_{os}=6$  (b),  $\Pi_{os}=9$  (c) and  $\Pi_{os}=12$  (d) for different values of  $\Pi_\gamma$ . The arrow denotes the increasing direction of  $\Pi_\gamma$ . NF record set.

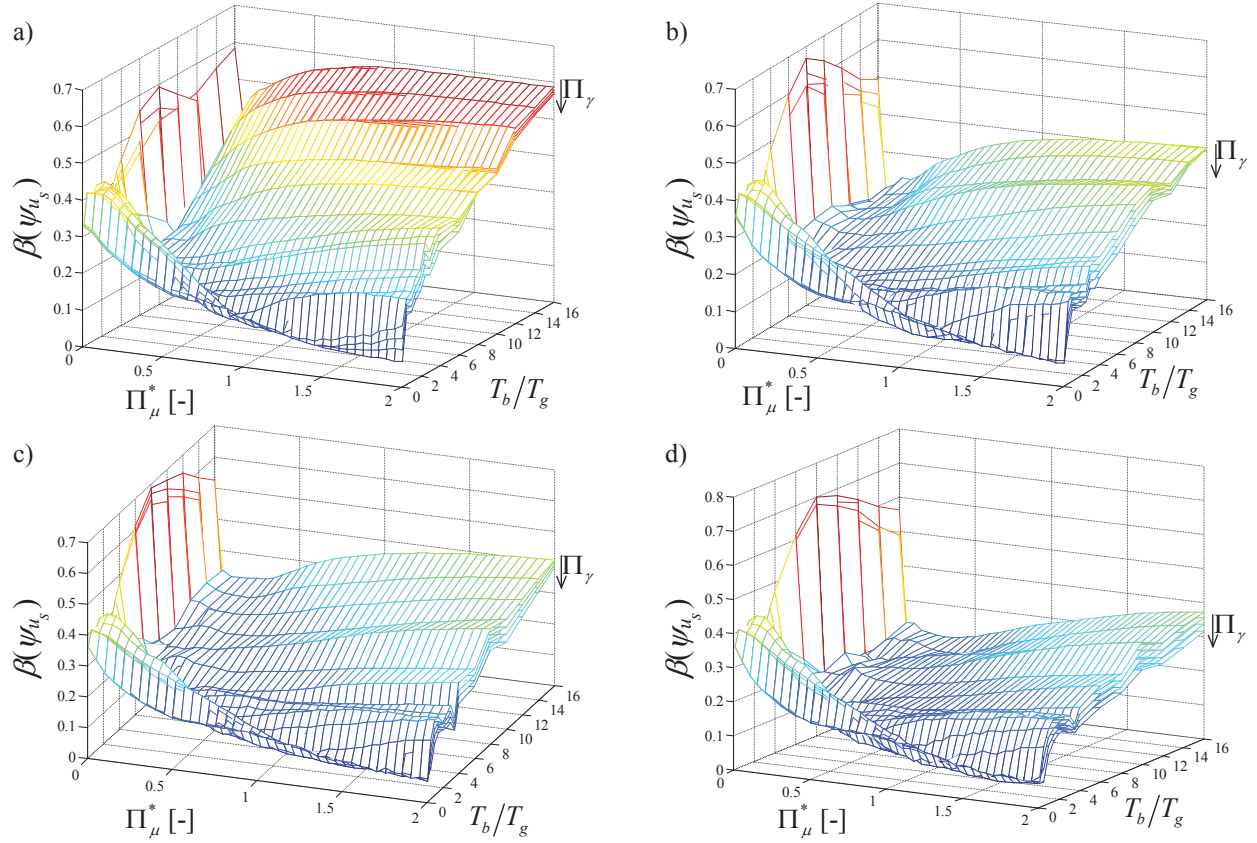


Fig. 11. Normalized superstructure displacement vs.  $\Pi_\mu^*$  and  $T_b/T_g$ : dispersion for  $\Pi_{os}=3$  (a),  $\Pi_{os}=6$  (b),  $\Pi_{os}=9$  (c) and  $\Pi_{os}=12$  (d) for different values of  $\Pi_\gamma$ . The arrow denotes the increasing direction of  $\Pi_\gamma$ . NF record set.

### Optimal sliding friction coefficient

The results reported in Figs. 5 and 10 show that for each combination of the system properties (i.e., of  $\Pi_\gamma$ ,  $\Pi_{\omega_s}$ ,  $\Pi_{\omega_b}$ ) there exists an optimal value of the normalized sliding friction coefficient,  $\Pi_{\mu,\text{opt}}^*$  such that the median (i.e., 50<sup>th</sup> percentile) normalized superstructure displacements are minimized. Fig. 12 and 13 show the variation of  $\Pi_{\mu,\text{opt}}^*$  with these parameters respectively in the case of FF records and NF records. The range of variation assumed for  $T_b/T_g$  is between 1 and 16. Values of  $T_b/T_g$  lower than 1 are not considered because they are not common in design practice, as the periods of vibration of isolated systems are generally higher than the values of  $T_g$  characteristic of seismic inputs.

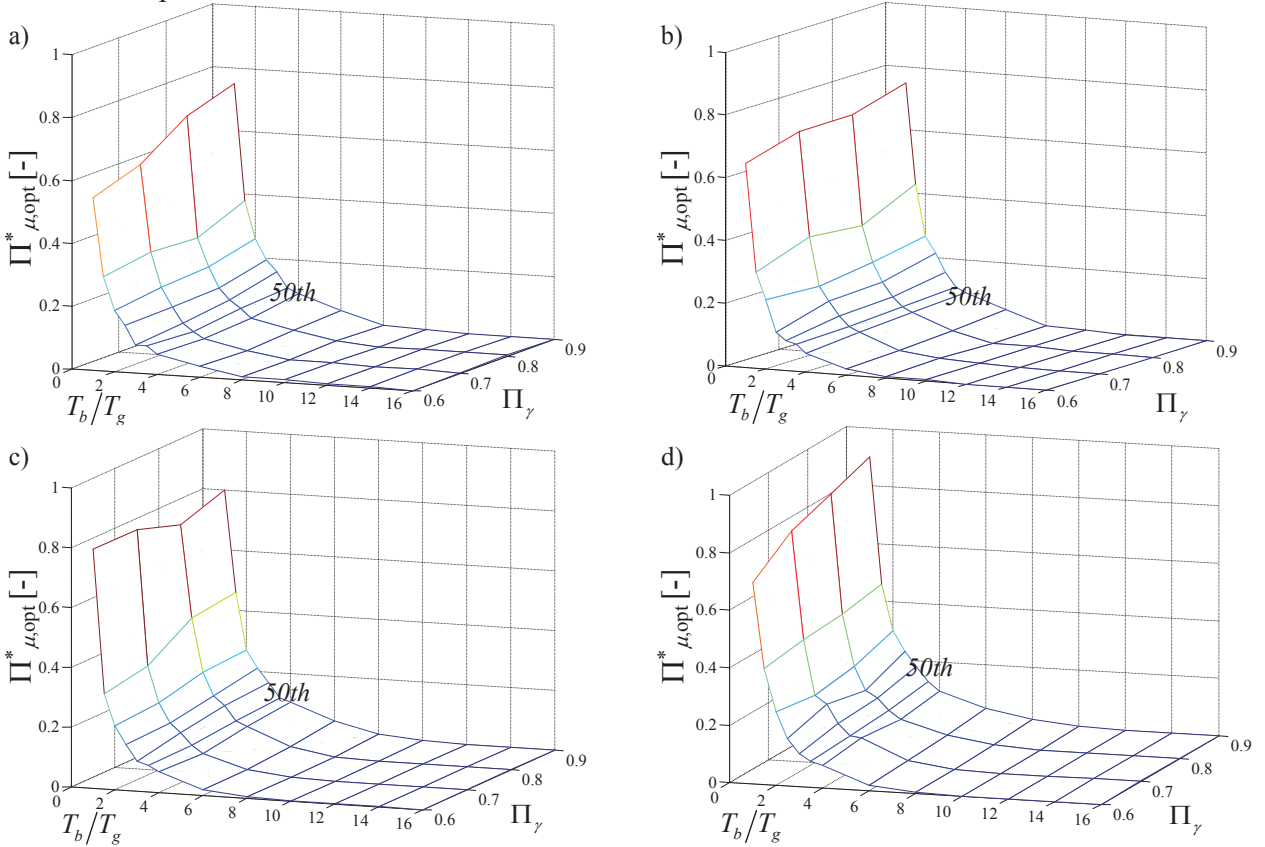


Fig. 12. Optimal values of normalized friction, that minimize the 50<sup>th</sup> percentile of the superstructure response, vs.  $\Pi_\gamma$  and  $T_b/T_g$  for  $\Pi_{\omega_s}=3$  (a),  $\Pi_{\omega_s}=6$  (b),  $\Pi_{\omega_s}=9$  (c) and  $\Pi_{\omega_s}=12$  (d). FF record set.

It is observed for both the FF and NF records that  $\Pi_{\mu,\text{opt}}^*$  generally increases by increasing  $\Pi_\gamma$  and by decreasing  $T_b/T_g$  whereas it does not show a clear and significant trend of variation with  $\Pi_{\omega_s}$ . The obtained results are consistent with those observed in Jangid [16] by considering a frame structure subjected to an earthquake input modeled as a stochastic process.

In order to give a better insight into the dependence of  $\Pi_{\mu,\text{opt}}^*$  on the  $T_b/T_g$  ratio, Fig. 14 reports the comparison between the median superstructure and isolator responses of two systems having different  $T_b/T_g$  ratio,  $\Pi_{\omega_s}=12$  and  $\Pi_\gamma=0.7$ , for  $T_g=1.03\text{s}$ , for the set of FF records. As already discussed previously, the superstructure displacements depend on the forces transmitted to the superstructure, which in turn depend on both the isolator displacement and the friction force. By increasing friction, the displacement reduces, but the friction force increases. Thus, there is an optimum amount of friction minimizing the superstructure response. The displacement reduction with  $\Pi_\mu^*$  is more significant for high  $T_b/T_g$  values than for low values (Fig. 14b) and this explains

why the optimum friction value is lower for high  $T_b/T_g$  values. Similar observations have been held for the case of NF records.

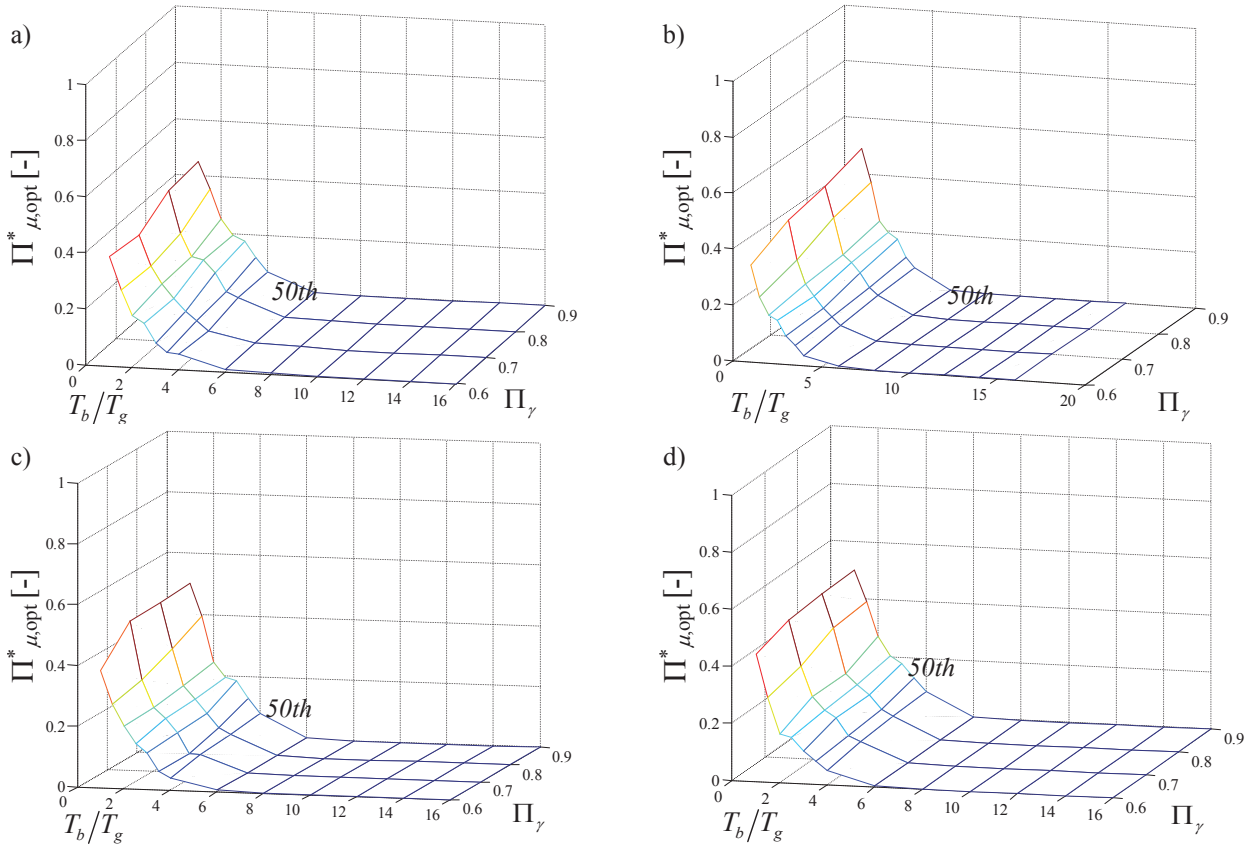


Fig. 13. Optimal values of normalized friction, that minimize the 50<sup>th</sup> percentile of the superstructure response, vs.  $\Pi_\gamma$  and  $T_b/T_g$  for  $\Pi_{os}=3$  (a),  $\Pi_{os}=6$  (b),  $\Pi_{os}=9$  (c) and  $\Pi_{os}=12$  (d). NF record set.

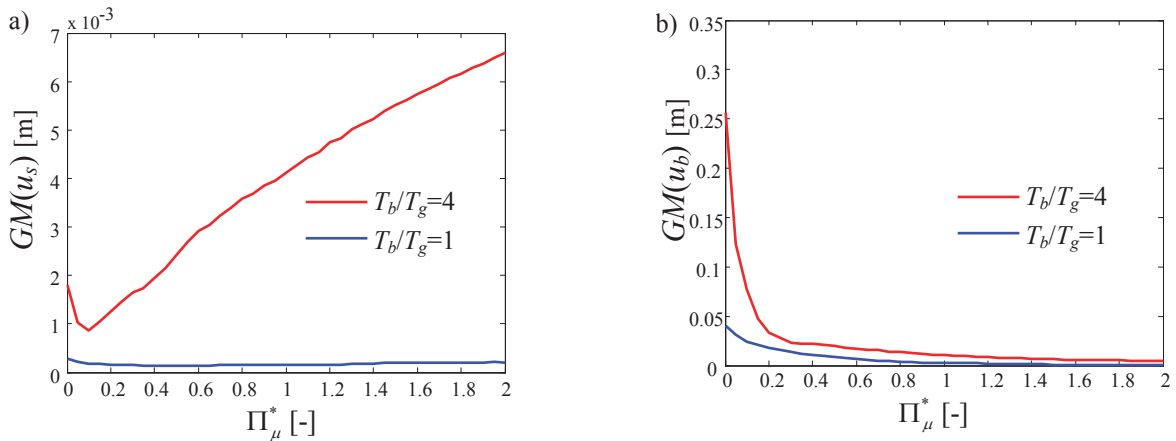


Fig. 14. Median superstructure displacement vs.  $\Pi^*_\mu$  (a), median bearing displacement vs.  $\Pi^*_\mu$  (b). FF records.

With regard to the dependency of the optimal friction on the type of records considered, it is observed that the values of  $\Pi^*_{\mu, opt}$  for the FF records are very similar to the values of  $\Pi^*_{\mu, opt}$  for the NF records, for values of  $T_b/T_g$  higher than 2 which are common in design practice.

From a design point of view, it may be of interest to evaluate the values of  $\Pi^*_{\mu, opt}$  that minimize response percentile others than the 50<sup>th</sup>, corresponding to different exceedance probabilities [51].

Fig. 15 and Fig. 16 show the trend of the optimal friction coefficient  $\Pi^*_{\mu, opt}$  that minimizes the 16<sup>th</sup> and 84<sup>th</sup> percentiles of the superstructure response under the FF records and the NF records respectively. As expected, higher values of  $\Pi^*_{\mu, opt}$  are required to minimize a higher percentile of the superstructure response.

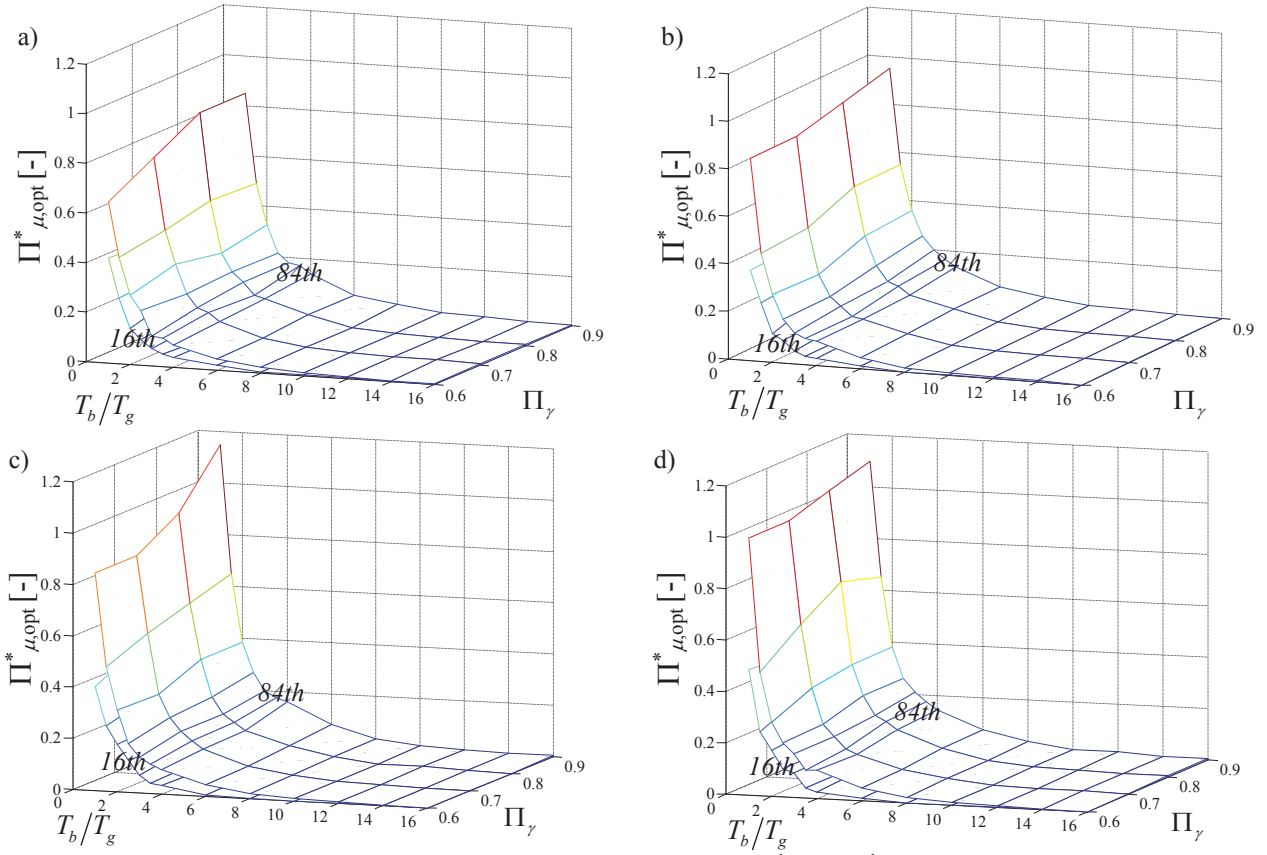


Fig. 15. Optimal values of normalized friction, that minimize the 16<sup>th</sup> and 84<sup>th</sup> percentiles of the superstructure response, vs.  $\Pi_\gamma$  and  $T_b/T_g$  for  $\Pi_{os}=3$  (a),  $\Pi_{os}=6$  (b),  $\Pi_{os}=9$  (c) and  $\Pi_{os}=12$  (d). FF record set.

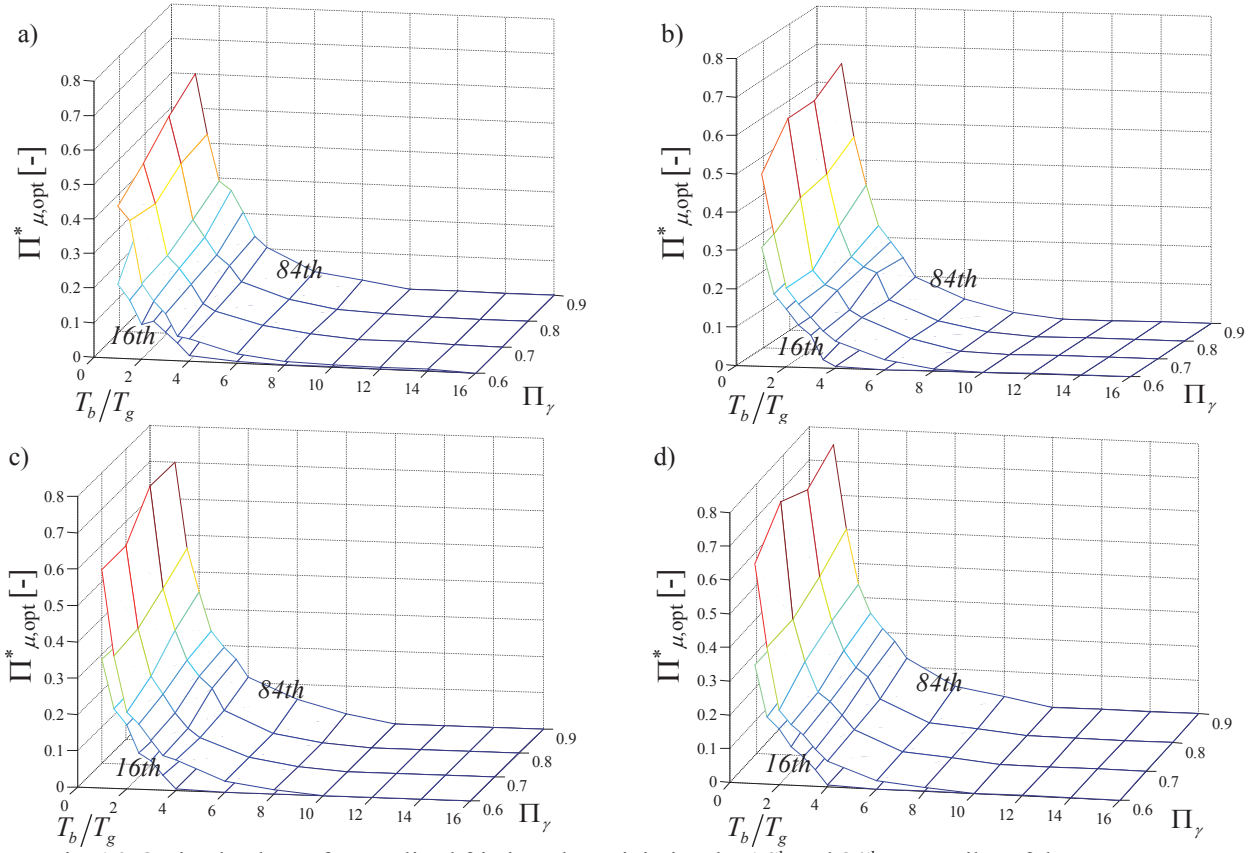


Fig. 16. Optimal values of normalized friction, that minimize the 16<sup>th</sup> and 84<sup>th</sup> percentiles of the superstructure response, vs.  $\Pi_\gamma$  and  $T_b/T_g$  for  $\Pi_{os}=3$  (a),  $\Pi_{os}=6$  (b),  $\Pi_{os}=9$  (c) and  $\Pi_{os}=12$  (d). NF record set.

The plots of Fig. 12,13,15,16 show that  $\Pi_{\mu,opt}^*$  is significantly influenced by  $\Pi_{\omega_g}$  whereas it is only slightly affected by  $\Pi_{\gamma}$  and  $\Pi_{\omega_s}$ . Moreover, the optimal values of the normalized friction coefficient are quite similar for the NF and FF records. Thus, the values of  $\Pi_{\mu,opt}^*$  are recomputed by considering the response samples from both the record sets for evaluating the response statistics and a linear regression analysis is carried out to obtain a closed-form expression for  $\Pi_{\mu,opt}^*$  as a function of  $\Pi_{\omega_g}$ , for the three percentile levels (i.e., 50<sup>th</sup>, 16<sup>th</sup> and 84<sup>th</sup> percentile). The regression formula is given the following form:

$$\Pi_{\mu,opt}^* = c_1 + c_2 \cdot \Pi_{\omega_g}^{-1} \geq 0 \quad (11)$$

where the parameters  $c_1$  and  $c_2$  are evaluated via Matlab [56].

Table 5 reports the values of the coefficients of the regression expression, characterized by R-squared values of 0.97, 0.90, 0.95 for the case of the 50<sup>th</sup>, 16<sup>th</sup> and 84<sup>th</sup> percentiles. These R-squared values are very high and they demonstrate the effectiveness of the proposed regression form and the high influence of  $\Pi_{\omega_g}$  on the results.

Table 5. Coefficients of regression for the optimal friction  $\Pi_{\mu,opt}^*$ .

	$c_1$	$c_2$
50 <sup>th</sup>	-0.0725	0.6386
84 <sup>th</sup>	-0.0545	0.7120
16 <sup>th</sup>	-0.0624	0.4897

Eqn.(11) can be used to design the optimum FPS properties for the isolated system, provided that the seismic intensity level  $PGA$  is assigned. In fact, according to Eqn.(6), the optimum friction coefficient (at high velocity) can be easily calculated as  $f_{max,opt} = \frac{\Pi_{\mu,opt}^* \cdot PGA}{g}$ . This implies that the optimum friction coefficient increases linearly with the  $IM$  level.

Fig. 17a reports the values of  $\Pi_{\mu,opt}^*$  for the case of the 50<sup>th</sup> percentile and the corresponding regression curve, whereas Fig. 17b reports and compares the regression curves for the three different percentiles considered.

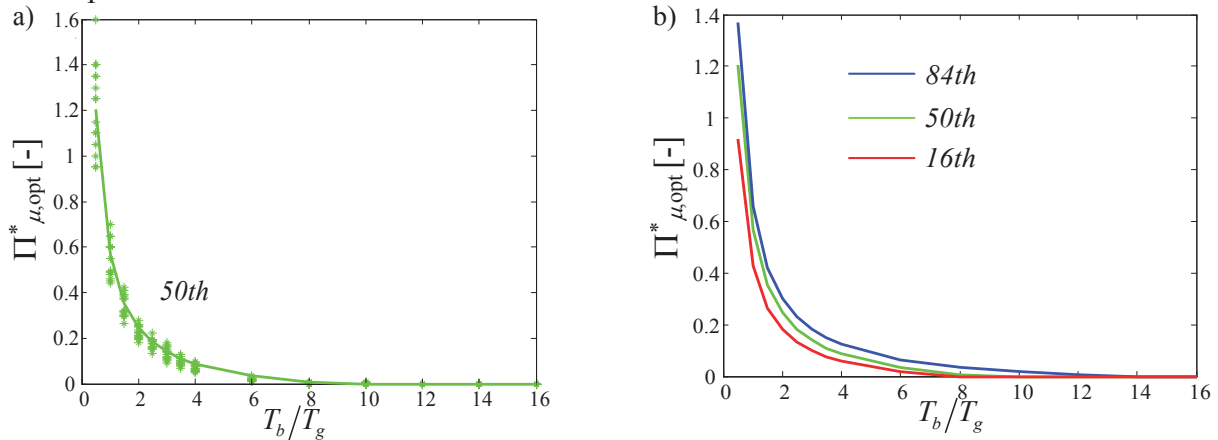


Fig. 17. Optimal values of normalized friction, that minimize the 50<sup>th</sup> percentile of the superstructure response vs.  $T_b/T_g$  compared to the corresponding regression curve (a), regression curves for the 50<sup>th</sup>, 16<sup>th</sup> and 84<sup>th</sup> percentile (b). Near fault and FF record set.

In Fig.17a it can be observed that the dispersion of the results, described by the scatter of the values of  $\Pi_{\mu,opt}^*$  with respect to the fitting curve, is quite high for low values of  $T_b/T_g$ , and it reduces for

increasing values of  $T_b/T_g$ . In order to reduce this dispersion, a multivariate linear regression analysis is carried out to obtain a closed-form expression for  $\Pi_{\mu,\text{opt}}^*$  by also accounting for the effect of the parameters  $\Pi_\gamma$ ,  $T_b/T_g$  and  $\Pi_{\omega_s}$  discarded in the previous regression. In particular, the following first-order polynomial expression considering the interaction between the terms is employed:

$$\Pi_{\mu,\text{opt}}^* = c_1 + c_2 \cdot \Pi_{\omega_g}^{-1} + c_3 \cdot \Pi_{\omega_s} + c_4 \cdot \Pi_\gamma + c_5 \cdot \Pi_{\omega_g}^{-1} \cdot \Pi_{\omega_s} + c_6 \cdot \Pi_{\omega_g}^{-1} \cdot \Pi_\gamma + c_7 \cdot \Pi_\gamma \cdot \Pi_{\omega_s} \geq 0 \quad (12)$$

where  $c_i$ ,  $i=1,\dots,7$ , are the regression coefficients, whose values are reported in Table 6 as a function of the different percentile levels. It is noteworthy that the order of the polynomials is kept as small as possible to balance the contrasting requirements of accuracy and simplicity, thus providing a polynomial expression easy to be applied for the preliminary designing of FPS characteristics. The regression R-squared values are higher than 0.9 for all the cases considered, and equal to 0.99 for the case of the 50<sup>th</sup> response percentile, indicating that the fitted model describes very well the variation of  $\Pi_{\mu,\text{opt}}^*$  with the parameters considered.

Table 6. Coefficients of multivariate non-linear regression for the optimal friction  $\Pi_{\mu,\text{opt}}^*$ .

	$c_1$	$c_2$	$c_3$	$c_4$	$c_5$	$c_6$	$c_7$
50th	-0.0242	0.2329	-0.0094	-0.0139	0.0252	0.2890	0.0057
84th	0.0433	0.0730	-0.0116	-0.0790	0.0279	0.5734	0.0086
16th	-0.1705	0.7187	-0.0046	0.1692	0.0125	-0.4298	0.0028

Multivariate nonlinear regression analysis is also carried out to find an expression for  $\psi_{u_s}(\Pi_{\mu,\text{opt}}^*)$  and  $\psi_{u_b}(\Pi_{\mu,\text{opt}}^*)$ , i.e., the normalized absolute value of the peak displacement demand of respectively the superstructure and isolation system corresponding to  $\Pi_{\mu,\text{opt}}^*$ , in function of  $\Pi_\gamma$ ,  $T_b/T_g$ ,  $\Pi_{\omega_s}$  for the three percentile levels considered. The expressions of  $\psi_{u_s}(\Pi_{\mu,\text{opt}}^*)$  and  $\psi_{u_b}(\Pi_{\mu,\text{opt}}^*)$  are:

$$\begin{aligned} \psi_u(\Pi_{\mu,\text{opt}}^*) = c_1 + c_2 \cdot \Pi_{\omega_g}^{-1} + c_3 \cdot \Pi_{\omega_s} + c_4 \cdot \Pi_\gamma + c_5 \cdot \Pi_{\omega_g}^{-1} \cdot \Pi_{\omega_s} + c_6 \cdot \Pi_{\omega_g}^{-1} \cdot \Pi_\gamma + c_7 \cdot \Pi_\gamma \cdot \Pi_{\omega_s} + \\ + c_8 \cdot \Pi_{\omega_g}^{-2} + c_9 \cdot \Pi_{\omega_s}^2 + c_{10} \cdot \Pi_\gamma^2 \geq 0 \quad u=u_s, u_b \end{aligned} \quad (13)$$

where  $c_i$ ,  $i=1,\dots,10$ , are the regression coefficients, whose values are reported in Tables 7 and 8, respectively, as a function of the different percentile levels. The regression R-squared values are higher than 0.9 for all the parameter values considered in the case of  $\psi_{u_s}(\Pi_{\mu,\text{opt}}^*)$  and higher than 0.8 in the case of  $\psi_{u_b}(\Pi_{\mu,\text{opt}}^*)$ .

Table 7. Coefficients of multi-variate non-linear regression for  $\psi_{u_s}(\Pi_{\mu,\text{opt}}^*)$ .

	$c_1$	$c_2$	$c_3$	$c_4$	$c_5$	$c_6$	$c_7$	$c_8$	$c_9$	$c_{10}$
50th	0.7880	0.0958	-0.1985	-0.1620	-0.0048	-0.0120	0.0360	-0.0022	0.0101	-0.0991
84th	1.1044	0.1536	-0.2803	-0.3585	-0.0083	-0.0200	0.0540	-0.0030	0.0145	-0.0631
16th	0.5420	0.0548	-0.1354	-0.0392	-0.0026	-0.0069	0.0243	-0.0014	0.0067	-0.1194

Table 8. Coefficients of multi-variate non-linear regression for  $\psi_{u_b}(\Pi_{\mu, \text{opt}}^*)$ .

	$c_1$	$c_2$	$c_3$	$c_4$	$c_5$	$c_6$	$c_7$	$c_8$	$c_9$	$c_{10}$
50th	-0.5101	1.0444	0.1065	0.3820	0.0056	0.0593	-0.0181	-0.0533	-0.0073	-1.0462
84th	-0.9976	1.4462	0.2591	0.1768	0.0158	-0.0431	-0.0968	-0.0577	-0.0167	-0.9508
16th	0.1200	0.5879	0.0739	-0.0472	0.0023	0.0436	-0.0195	-0.0338	-0.0042	-0.3874

## CONCLUSIONS

This study has investigated the relation between the ground motion characteristics and the optimal friction pendulum (FP) bearings properties for the seismic isolation of structural systems. The ground motion characteristics have been synthetically described by the peak ground acceleration (PGA) and the parameter  $T_g$  related to the peak ground acceleration-to-velocity (PGA/PGV) ratio.

These parameters have been employed to develop a non-dimensional formulation for evaluating the seismic behavior of a two-degree-of-freedom model representative of the isolated system, by considering two different families of records representative respectively of near fault and far field seismic inputs.

The result of the seismic analyses, carried out for different values of the non-dimensional parameters characteristic of the problem, show that:

- the PGA is not an efficient seismic intensity measure for the problem at hand, and the parameter  $T_g$  should also be considered to achieve a more confident estimate of the response;
- the ratio  $T_b / T_g$  between the undamped fundamental circular frequency of the isolated system and the ground motion period affects significantly the response.
- the geometric mean of the normalized isolator response first increases for increasing  $T_b / T_g$  and then it decreases, whereas the geometric mean of the normalized superstructure response increases for increasing values of  $T_b / T_g$ .
- for the same values of the non-dimensional parameters characteristic of the system and of the ground motion, the normalized responses under far field (FF) and near fault (NF) records are quite similar to each other. FF records induce slightly higher displacement demands because differently from NF records they are characterized by multiple cycles of large amplitudes rather than a single pulse.
- there exists an optimal value of the normalized friction that minimizes the normalized superstructure displacement response. This optimal value is significantly affected by and inversely proportional to  $T_b / T_g$ , and only slightly affected by the other non-dimensional parameters.

In the final part of the paper, regression expressions, characterized by different order and accuracy, have been derived for the optimal values of the normalized friction coefficient minimizing the 50<sup>th</sup>, 16<sup>th</sup> and 84<sup>th</sup> percentile values of the superstructure normalized displacements, as function of the identified system characteristic parameters and ground motion parameters. These equations can be very useful for the preliminary design of the optimal FP properties by also accounting for the influence of the ground motion characteristics.

## REFERENCES

- [1] Naeim F, Kelly JM. Design of seismic isolated structures: from theory to practice. New York: John Wiley and Sons; 1999.
- [2] Christopoulos C, Filiatrault A. *Principles of Passive Supplemental Damping and Seismic Isolation*. IUSS Press: Pavia, Italy, 2006.
- [3] Fenz, D. M., & Constantinou, M. C. (2006). Behaviour of the double concave friction pendulum bearing. *Earthquake Engineering & Structural Dynamics*, 35(11), 1403-1424.

- [4] Mosqueda G, Whittaker AS, Fenves GL. Characterization and modeling of Friction Pendulum bearings subjected to multiple components of excitation. *Journal of Structural Engineering* 2004; **130**(3):433-442.
- [5] Mokha A, Constantinou MC, Reinhorn AM. Teflon Bearings in Base Isolation. I: Testing. *Journal of Structural Engineering* 1990; **116**(2):438-454.
- [6] Constantinou MC, Mokha A, Reinhorn AM. Teflon Bearings in Base Isolation. II: Modeling. *Journal of Structural Engineering* 1990; **116**(2):455-474.
- [7] Constantinou MC, Whittaker AS, Kalpakidis Y, Fenz DM, Warn GP. Performance of Seismic Isolation Hardware Under Service and Seismic Loading. *Technical Report MCEER-07-0012*, 2007.
- [8] Almazàn JL, De la Llera JC. Physical model for dynamic analysis of structures with FPS isolators. *Earthquake Engineering and Structural Dynamics* 2003; **32**(8):1157–1184.
- [9] Landi, Luca, Gianluca Grazi, and Pier Paolo Diotallevi. "Comparison of different models for friction pendulum isolators in structures subjected to horizontal and vertical ground motions." *Soil Dynamics and Earthquake Engineering* 81 (2016): 75-83.
- [10] Ryan KL, Chopra AK. Estimating the seismic displacement of friction pendulum isolators based on non-linear response history analysis. *Earthquake Engineering and Structural Dynamics* 2004; **33**(3): 359–373.
- [11] Barroso LR. Performance evaluation of vibration controlled steel structures under seismic loads. PhD thesis, Stanford University, California, US, 1999.
- [12] Barroso LR, Winterstein S. Probabilistic seismic demand analysis of controlled steel moment-resisting frame structures. *Earthquake Engineering and Structural Dynamics* 2002; **31**(12): 2049–2066.
- [13] Landi L., Grazi G., Diotallevi P. P. Comparison of different models for friction pendulum isolators in structures subjected to horizontal and vertical ground motions, *Soil Dynamics and Earthquake Engineering*, 2016;81: 75–83.
- [14] Constantinou, M. C., & Tadjbakhsh, I. G. (1984). The optimum design of a base isolation system with frictional elements. *Earthquake engineering & structural dynamics*, 12(2), 203-214.
- [15] Jangid RS. Optimum frictional elements in sliding isolation systems. *Computers and Structures* 2000; **76**(5): 651–661.
- [16] Jangid RS. Optimum friction pendulum system for near-fault motions. *Engineering Structures* 2005; 27(3): 349–359.
- [17] Fragiaco, M., Rajgelj, S., & Cimadam, F. (2003). Design of bilinear hysteretic isolation systems. *Earthquake engineering & structural dynamics*, 32(9), 1333-1352.
- [18] Iemura H, Taghikhany T, Jain S. Optimum design of resilient sliding isolation system for seismic protection of equipments. *Bulletin of Earthquake Engineering* 2007; **5**(1):85–103.
- [19] Chung LL, Kao PS, Yang CY, Wu LY, Chen HM. Optimal frictional coefficient of structural isolation system. *Journal of Vibration and Control* 2013, Early view. DOI: 10.1177/1077546313487938.
- [20] Castaldo, P, Tubaldi, E. Influence of fps bearing properties on the seismic performance of base-isolated structures. *Earthquake Engineering and Structural Dynamics* 2015; **44**(15):2817–2836.
- [21] Castaldo P, Palazzo B, Della Vecchia P. Seismic reliability of base-isolated structures with friction pendulum bearings. *Engineering Structures* 2015; **95**: 80-93.
- [22] Castaldo P., Amendola G., Palazzo B., Seismic fragility and reliability of structures isolated by friction pendulum devices: seismic reliability-based design (SRBD), *Earthquake Engineering and Structural Dynamics*, **46**(3); 425–446, DOI: 10.1002/eqe.2798.
- [23] Bucher C. Probability-based optimization of friction-based seismic isolation devices. *Structural Safety* 2009; **31**(6): 500–507.
- [24] Castaldo P., Palazzo B., Della Vecchia P. Life-cycle cost and seismic reliability analysis of

- 3D systems equipped with FPS for different isolation degrees, *Engineering Structures*, 2016; 125:349–363. DOI:10.1016/j.engstruct.2016.06.056.
- [25] Chara Ch. Mitropoulou and Nikos D. Lagaros Life-Cycle Cost Model and Design Optimization of Base-Isolated Building Structures, *Frontiers in Built Environment*, 2016(2); 1-15, doi: 10.3389/fbuil.2016.00027.
- [26] Inaudi, J. A., & Kelly, J. M. (1993). Optimum damping in linear isolation systems. *Earthquake engineering & structural dynamics*, 22(7), 583-598.
- [27] Dicleli, M., & Buddaram, S. (2006). Effect of isolator and ground motion characteristics on the performance of seismic-isolated bridges. *Earthquake engineering & structural dynamics*, 35(2), 233-250.
- [28] Liao, W. I., Loh, C. H., & Lee, B. H. (2004). Comparison of dynamic response of isolated and non-isolated continuous girder bridges subjected to near-fault ground motions. *Engineering Structures*, 26(14), 2173-2183.
- [29] Hameed, A., Koo, M. S., Dai Do, T., & Jeong, J. H. (2008). Effect of lead rubber bearing characteristics on the response of seismic-isolated bridges. *KSCE Journal of Civil Engineering*, 12(3), 187-196.
- [30] Castaldo P., Ripani M. Optimal design of friction pendulum system properties for isolated structures considering different soil conditions. *Soil Dynamics and Earthquake Engineering* 2016; 90:74–87. DOI:10.1016/j.soildyn.2016.08.025.
- [31] Vassiliou F M, Tsiavos A, Stojadinović B. Dynamics of inelastic base-isolated structures subjected to analytical pulse ground motions. *Earthquake Engineering & Structural Dynamics*, 2013;42(14): 2043–2060.
- [32] Zhu, T.J., Tso, W.K., and Heidebrecht, A.C. (1988). “Effect of peak ground A/V ratio on structural damage.” *Journal of Structural Engineering*, Vol. 114, pp. 1019–1037.
- [33] Tso, W. K., Zhu, T. J., & Heidebrecht, A. C. (1992). Engineering implication of ground motion A/V ratio. *Soil Dynamics and Earthquake Engineering*, 11(3), 133-144.
- [34] Sawada T, Hirao K, Yamamoto H, Tsujihara O. Relation between maximum amplitude ratio and spectral parameters of earthquake ground motion. In: Proc. 10th world conf. on earthquake engineering, vol. 2. 1992, p. 617–22.
- [35] F. Pavel & D. Lungu (2013) Correlations Between Frequency Content Indicators of Strong Ground Motions and PGV, *Journal of Earthquake Engineering*, 17:4, 543-559, DOI: 10.1080/13632469.2012.762957.
- [36] Jafarian, Y., Kermani, E., & Baziar, M. H. (2010). Empirical predictive model for the  $v_{max}/a_{max}$  ratio of strong ground motions using genetic programming. *Computers & Geosciences*, 36(12), 1523-1531.
- [37] Occhiuzzi A, Veneziano D, Van Dyck J. Seismic Design of Base Isolated Structures. Second International Conf. on Earthquake Resistant Construction and Design, Berlin, Germany, 1994, 541-548.
- [38] Vassiliou MF, Tsiavos A, Stojadinović B. Dynamics of inelastic base-isolated structures subjected to analytical pulse ground motions. *Earthquake Engineering and Structural Dynamics* 2013; 42:2043–2060.
- [39] Castaldo P., Palazzo B. and Ferrentino T. Seismic reliability-based ductility demand evaluation for inelastic base-isolated structures with friction pendulum devices, *Earthquake Engineering and Structural Dynamics* 2016, DOI: 10.1002/eqe.2854.
- [40] Rathje, E. M., Faraj, F., Russell, S., and Bray, J. D. (2004). “Empirical relationships for frequency content parameters of earthquake ground motions.” *Earthquake Spectra*, 20(1), 119–144.
- [41] Makris, N., and Black, C. J. (2004a). “Dimensional analysis of bilinear oscillators under pulse-type excitations.” *J. Eng. Mech.*, 130(9), 1019–1031.
- [42] Karavasilis TL, Seo CY, Makris N. Dimensional Response Analysis of Bilinear Systems Subjected to Non-pulse like Earthquake Ground Motions. *Journal of Structural Engineering*

2011; **137**(5): 600–606.

- [43] Dimitrakopoulos, E., Kappos, A. J., & Makris, N. (2009). Dimensional analysis of yielding and pounding structures for records without distinct pulses. *Soil dynamics and earthquake engineering*, 29(7), 1170-1180.
- [44] Málaga-Chuquitaype, C. (2015). Estimation of peak displacements in steel structures through dimensional analysis and the efficiency of alternative ground-motion time and length scales. *Engineering Structures*, 101, 264-278.
- [45] Katsanos, E. I., Sextos, A. G., & Manolis, G. D. (2010). Selection of earthquake ground motion records: A state-of-the-art review from a structural engineering perspective. *Soil Dynamics and Earthquake Engineering*, 30(4), 157-169.
- [46] Iervolino I, Galasso C, Cosenza E. REXEL: computer aided record selection for code-based seismic structural analysis. *Bull Earthquake Eng* 2010; **8**(2):339–362.
- [47] Porter KA. An overview of PEER’s performance-based earthquake engineering methodology. Proceedings, *Proceedings of the 9th International Conference on Application of Statistics and Probability in Civil Engineering (ICASP9)*, San Francisco, California, 2003.
- [48] Shome N, Cornell CA, Bazzurro P, Carballo JE. Earthquake, records, and nonlinear responses. *Earthquake Spectra* 1998; **14**(3): 469-500.
- [49] Luco N, Cornell CA. Structure-specific scalar intensity measures for near-source and ordinary earthquake ground motions. *Earthquake Spectra* 2007; **23**(2): 357-92.
- [50] Pinto PE, Giannini R, Franchin P. *Seismic Reliability Analysis of Structures*, IUSS Press, Pavia, Italy, 2003.
- [51] Ryan K, Chopra A. Estimation of Seismic Demands on Isolators Based on Nonlinear Analysis. *Journal of Structural Engineering* 2004; **130**(3): 392–402.
- [52] Mollaioli F, Lucchini A, Cheng Y, Monti G. Intensity measures for the seismic response prediction of base-isolated buildings. *Bulletin of Earthquake Engineering* 2013; **11**(5): 1841–1866.
- [53] Barbato M, and Tubaldi E. A probabilistic performance-based approach for mitigating the seismic pounding risk between adjacent buildings. *Earthquake Engineering & Structural Dynamics*, 2013; **42**(8): 1203–1219.
- [54] Karavasilis T, Seo C. Seismic structural and non-structural performance evaluation of highly damped self-centering and conventional systems. *Engineering Structures* 2011, **33**(8): 2248-2258.
- [55] Cornell C, Jalayer F, Hamburger R, Foutch D. Probabilistic Basis for 2000 SAC Federal Emergency Management Agency Steel Moment Frame Guidelines. *Journal of Structural Engineering* 2002; **128**(4): 526-533.
- [56] Math Works Inc. MATLAB-High Performance Numeric Computation and Visualization Software. User’s Guide. Natick: MA, USA, 1997.
- [57] Ang AHS, Tang WH. Probability Concepts in Engineering-Emphasis on Applications to Civil and Environmental Engineering. John Wiley & Sons, New York, USA, 2007.
- [58] Jafarian, Y., Kermani, E., & Baziar, M. H. (2010). Empirical predictive model for the  $v_{max}/a_{max}$  ratio of strong ground motions using genetic programming. *Computers & Geosciences*, 36(12), 1523-1531.
- [59] Jangid R. S., Kelly J. M. Base isolation for near-fault motions. *Earthquake Engineering and Structural Dynamics* 2001, 30:691-707.
- [60] Mazza F., Vulcano A. Nonlinear Response of RC Framed Buildings with Isolation and Supplemental Damping at the Base Subjected to Near-Fault Earthquakes. *Journal of Earthquake Engineering* 2009, 13(5):690-715.
- [61] Chopra, A. K., & Chintanapakdee, C. (2001). Comparing response of SDF systems to near-fault and far-fault earthquake motions in the context of spectral regions. *Earthquake Engineering & Structural Dynamics*, 30(12), 1769-1789.

**Highlights:**

1. Influence of ground motion parameters on performance of systems isolated by FPS;
2. PGA/PGV assumed as representative of ground motion frequency characteristics;
3. Nondimensionalization of the equations of motion in function of PGA and PGA/PGV;
4. Response to both near-fault and far-field earthquakes is investigated;
5. Regression expressions accounting for effect of PGA/PGV on optimal friction;